Velocity Inversion by Coherency Optimization

W. W. Symes
J. J. Carrazzone

CRPC-TR89014
March 1989

Center for Research on Parallel Computation
Rice University
P.O. Box 1892
Houston, TX 77251-1892

Velocity Inversion by Coherency Optimization

W.W. Symes
Department of Mathematical Sciences
Rice University
Houston, Texas

J.J. Carazzone
Long-Range Research
Exxon Production Research Company
Houston, Texas

March 1989

Acknowledgement. This research was partly supported by the Office of Naval Research under contracts N00014-85-K0725 and N00014-89-J-1115, and by the National Science Foundation under grant DMS 86-03164 (W.W. Symes). Computations were performed at the Cray XMP facility of the Naval Research Laboratory. We are grateful for the permission of Exxon Production Research Company to publish the results based on the field data, and to allow the participation of J.J. Carazzone.

Abstract

We introduce an approach to velocity and reflectivity estimation based on optimizing the coherence of multiple shot-gathering inversions of reflection seismograms. The resulting algorithm appears to avoid severe convergence difficulties reported for output (nonlinear) least-squares inversion. We describe in detail an algorithm appropriate for plane-layered acoustic models, using the convolutional approximation to the plane-wave (p-tau) seismogram. We give theoretical and numerical evidence that coherency optimization, as defined here, yields stable and reasonably accurate estimates of both velocity trend and reflectivity, by exploiting reflection phase moveout and amplitudes in a computationally efficient way. We demonstrate that the approach may be applied to field data by extracting velocity and reflectivity estimates from a Gulf of Mexico marine data set. Finally we explain briefly how the approach may be modified to determine elastic models and source parameters as well as to determine laterally heterogeneous models.

1 Introduction

Full waveform inversion algorithms for multi-offset seismic reflection data have been discussed extensively over the past several years. For a small sample of this discussion, see Bamberger *et al.* (1982), Lines and Treitel (1984), Tarantola (1984, 1986), Gauthier *et al.* (1986), MacAulay (1985), Kolb *et al.* (1986), Mora (1986, 1987), Pan *et al.* (1988), Pan and Phinney (1989), Cao *et al.* (1989). All of the work just cited is based on the *output least-squares principle* in which a physical model of the subsurface is adjusted to minimize the mean square error between model-predicted and data seismograms. This approach does not require picked travel-times, unlike reflection tomography (Bube *et al.* (1985), Lines *et al.* (1987)) and in principle can extract seismic velocity estimates as well as reflection amplitudes, unlike linearized inversion (Cohen and Bleistein (1979), Clayton and Stolt (1981), Beylkin (1985), Ikelle *et al.* (1988), Beylkin and Burridge (1987)). In addition, any desired level of physical detail may be built into the output least-squares principle, and it may also incorporate non-seismic constraints (Lines *et al.* (1988)). Accordingly, some motivations for the interest in model-based full wave-form inversion are the possibilities of more-or-less automatic determination of complicated seismic velocity structures, and of rational extraction of reflection characteristics directly indicating the presence of hydrocarbon deposits.

In practice it has proven difficult to realize the promise of output least-squares inversion, even for synthetic data sets. The hypersensitivity of the reflection seismogram to slowly varying velocity components results in severe non-convexity of the mean-square-error, and consequent slow, or no, convergence of the (necessarily iterative) solution algorithms. Despite some progress for layered models (Kolb *et al.* (1986), Canadas and Kolb (1986), MacAulay (1986), Cao *et al.* (1989)), in general quite accurate initial estimates of velocity are required, else the amplitude preserving depth-migration function is disabled as well (Gauthier *et al.* (1986), Mora (1987), Pan and Phinney (1989), Ikelle *et al.* (1988), Tarantola (1986), Santosa and Symes (1989), Spratt (1987)). That is, for essentially mathematical reasons, least-squares inversion generally fails to give reliable velocity and reflectivity estimates.

The purpose of this paper is to introduce a variant of output-least-squares

inversion which appears to have better mathematical properties than does the straightforward version. This variant is based on optimizing the coherence of multiple inversions, so we call it the *coherency method.* The essential idea is very old, and is operative in ordinary (NMO-based) velocity analysis and in more speculative iterative before-stack migration schemes. Our specific quantification of coherence seems to be novel, and leads to a large class of algorithms, which we begin to explore in this and related papers.

The simple version of the coherency method used in this paper is based on a model of the plane-wave (p-tau) seismogram. Two hypotheses explain the essence of the model, and also hint at its limitations.

i) Each (plane-wave) trace is the convolution of a primary reflectivity with a source wavelet (plus noise).

ii) The reflectivities for various slownesses (or incidence angles) are related in the manner appropriate for a layered acoustic model.

The first assumption is that each trace can be explained by the venerable *convolutional model.* Thus multiple reflections are neglected. The second hypothesis makes explicit the layered medium assumption, already implicit in (i), and also restricts the change in reflectivity amplitude with angle to that appropriate to a layered fluid.

We shall establish three major points in this paper: First, a variational principle extracted from the above hypotheses (Section 3) is *convex* over a large region in model space. In particular, when coupled with suitable numerical optimization software, it yields the only waveform inversion algorithm known to the authors capable of reliable estimation of velocity (trends, i.e. long wavelengths) starting from grossly incorrect initial estimates. We illustrate this feature via a synthetic example (Section 4). Mathematically rigorous arguments leading to similar conclusions are presented in companion papers, referenced below.

Second, the coherency method is *practical*, in the sense that it can be applied to field data sets and — at least sometimes — produces reasonable results. We process a plane-wave gather derived from a marine survey in the Gulf of Mexico, using the implementation of the coherency method mentioned above (Section 5). This data set was selected and processed to conform as

closely as possible to the hypotheses underlying the current implementation (i.e. (i) and (ii) above). The velocities and reflectivities obtained compare favorably to those evident in a sonic log from a well near the line.

Third, the coherency method may be formulated for laterally heterogeneous models, for variable-density or elastic (rather than acoustic) models, and using the fully nonlinear model-data relationship rather than the convolutional model or analogous higher-dimensional linearized approximations. In particular, the coherency method is no more restricted to analysis of layered systems than is output-least-squares inversion. This point is of critical importance, as the central issue in velocity analysis is reliable and accurate estimation of laterally heterogeneous velocities. We describe explicitly a formulation based on shot gathers, designed to extract laterally heterogeneous velocities and reflectivities in the acoustic model (Section 6).

1 Output Least-squares Inversion

The discussion in this and the following three sections is based on the convolutional approximation to the plane-wave seismogram over a plane-layered acoustic earth model with constant density. Thus the only mechanical variation allowed in this model is the compressional velocity profile $c(z)$. While this model underlies a great deal of seismic data processing, it is clearly a gross simplification of seismic wave mechanics. Some of the concepts discussed below are extended to more realistic models in Section 6. The mathematical essence of velocity inversion is already present in the very simple plane-layer context, however, so we first develop the solution of the problem in that context. For discussion of plane-wave seismograms, and their production from synthetic point-source data and field reflection data, see Gutowski *et al.* (1982) and Brysk (1986).

Denote the plane-wave ("p-τ") seismogram corresponding to a velocity profile $c(z)$ by $S[c]$. The arguments in this paper are based on the well-known convolutional approximation, which is reasonably accurate when c may be re-written as a sum

$$c \approx c_s + c_r$$

where

$c_s(z)$ is a slowly varying background velocity model

$c_r(z)$ is a rapidly varying "reflector sequence," having locally zero mean on the length scale of significant change in the background velocity.

Thus the (two-way) travel-time to depth z of a precritical plane-wave at (horizontal) slowness p is determined with a small error by the background velocity $c_s(z)$ according to

$$\tau(z,p) = 2\int_0^z dz' \left(\frac{1}{c_s^2(z)} - p^2\right)^{1/2} = 2\int_0^z \frac{1}{v_s}$$

where v_s is the vertical (plane-wave) velocity at slowness p:

$$\begin{aligned} v_s(z,p) &= \left(\frac{1}{c_s^2(z)} - p^2\right)^{-1/2} = c_s(z)\Lambda(z,p) \\ \Lambda(z,p) &= (1 - c_s^2(z)p^2)^{-1/2}. \end{aligned}$$

The convolutional approximation to the plane-wave seismogram with (possibly directionally-dependent, known) source wavelet $f(t,p)$ is then

$$\begin{aligned} S[c_s, c_r](t,p) &= f * \frac{\partial r}{\partial t}(t,p) \\ &= \int_0^t dt' f(t-t',p)\frac{\partial r}{\partial t}(t',p) \end{aligned} \tag{1}$$

where the "reflectivity" $r(t,p)$ is given by

$$r(t,p) = \frac{v_r(\zeta(t,p),p)}{v_s(\zeta(t,p),p)} \tag{2}$$

by means of the *inverse two-way travel-time* function ζ, defined implicitly by

$$t = 2\int_0^{\zeta(t,p)} \frac{1}{v_s},$$

and the vertical velocity perturbation

$$v_r = c_r \cdot \Lambda^3.$$

Note that reflectivity conventionally means $\partial r/\partial t$; we shall confuse r and its t-derivative, calling both "reflectivity" as convenient. Note also that all surface-related phenomena, as well as source and receiver characteristics, are subsumed in the source wavelet $f(t,p)$. A detailed derivation of this model, appropriate to linear acoustics, may be found in Santosa and Symes (1988).

Now S is clearly linear in c_r, but quite nonlinear in c_s. In fact, a change in c_s will typically result in a change in the "phase" ζ, and thus in a *shift* in the high-frequency components of S, which in turn derive from the high-frequency components in c_r. Since such a phase-shift may have a drastic effect on components of the appropriate (high) frequency. Since c_r must have a great deal of high-frequency content in order to model the dense distribution of reflectors in the typical sedimentary column, one expects S to be extremely sensitive to changes in the background velocity c_s.

This oversensitivity to background errors shows quite clearly in the expression for the perturbation δS in the seismogram, due to a perturbation δc_s in the background velocity (holding c_r fixed, and assuming $\delta c_s(0) = 0$):

$$\delta S(t,p) = f * \frac{\partial}{\partial t}\left(-\frac{v_r}{v_s^2}\delta v_s + \frac{\partial}{\partial z}(\frac{v_r}{v_s})\delta\tilde{\zeta}\right)(\zeta(t,p),p)$$

where

$$\delta\tilde{\zeta}(z,p) := \delta\zeta(\tau(z,p),p) = v_s(z,p)\int_0^z dz' v_s(z',p)c_s^{-3}(z')\delta c_s(z')$$

is the phase perturbation corresponding to δc_s, referred to depth/slowness coordinates.

Thus the second derivative of c_r (or, of r) appears in the perturbations δS associated with a background velocity perturbation δc_s. On the other hand, a perturbation δc_r in c_r simply results in

$$\delta S \sim S[c_s, \delta c_r]$$

as S is linear in the derivative of c_r. Thus δS is linear in the derivative of δc_r.

Again, c_r must be highly oscillatory to model the typical reflector distribution, so the second derivative of c_r is typically much bigger, in any

reasonable sense, than is the first derivative of c_r itself. Thus perturbation of the background velocity c_s has a much larger effect on S than does perturbation of c_r: in the language of linear algebra, the linear perturbation map ("Jacobian")

$$\delta c_s,\ \delta c_r \mapsto \delta S$$

is *ill-conditioned.*

Even worse, a straighforward extension of this reasoning shows that the difference between the perturbed seismogram

$$S[c_s + \delta c_s, c_r + \delta c_r]$$

and its linear prediction

$$S[c_s, c_r] + \delta S$$

can easily be on the order of S itself, even for quite small δc_s.

To summarize: under realistic assumptions on c_s and c_r,

(i) the Jacobian δS is ill-conditioned;

(ii) S is poorly approximated by its linearization.

Consequently, the output least-squares objective function

$$J_{LS}[c_s, c_r; S_{data}] := \int\int dp\, dt |S[c_s, c_r] - S_{data}|^2$$

is highly non-convex, with rapidly changing gradient.

To illustrate these features of the mean-square error function, we constructed the convolutional plane-wave (reference) seismogram (Figure 2) corresponding to a (reference) model (velocity profile) of the form: smooth background (c_s) plus rough reflector series (c_r) (Figure 1).

Remark. We have elected to calibrate all velocities in units of surface velocity, so that $c_s(0) = 1$ always, and correspondingly to measure depth (z) in seconds of one-way time at surface velocity. This normalization has a salubrious effect on the scaling of various numerical computations; physical units can easily be recovered when desired.

We added multiples of a trend perturbation $\delta c_s(z)$ (Figure 3) to $c_s(z)$. We produced for each value h in the range $0 \leq h \leq 1.2$ the seismogram corresponding to the perturbed background velocity

$$c_s(z) + (h-1)\delta c_s(z)$$

with in all cases the same reflector series $c_r(z)$. Note that these are *finite* perturbations, and that for $h = 0$ the perturbed velocity profile is constant (independent of z). Next we subtract the seismogram for $h = 1$ from the seismogram computed for each value of h, and form the mean-square of the resulting difference (i.e. a suitably discretized version of):

$$\int_0^{t_{max}} \int_0^{p_{max}} dt\, dp |S[c_s + (h-1)\delta c_s, c_r](t,p) - S[c_s, c_r](t,p)|^2$$

This quantity is plotted *versus* the parameter h in Figure 4. This figure represents a sampling of the mean-square error — the objective function of output least squares — along a line segment in model space connecting the homogeneous background ($h = 0$) with the reference background ($h = 1$), with the reference seismogram playing the role of the data gather.

The features mentioned above are evident in Figure 4: the mean square error changes rapidly near the "solution" ($h = 1$), and possesses many local minima and maxima. Near the homogeneous background velocity ($h = 0$), which might be selected as a natural "initial guess," the *local* trend of the mean square error bears no particular relation to the *global* trend. Consequently, relatives of Newton's method have little prospect of success in finding the global minimum. Examples of the failure of Newton-type methods started at a poor (but reasonable) initial guess are presented in Kolb *et al.* (1986), Gauthier *et al.* (1986), Santosa and Symes (1989). Remedies for this delinquent behavior have been suggested by Kolb *et al.* (1986), Cao *et al.* (1989), MacAulay (1986). None of these remedies change the basic character of the objective function: highly nonconvex, with rapidly varying gradient. Since methods based on local behaviour of the objective, exemplified by Newton's method, are virtually mandated by the size of the seismic inverse problem, especially for laterally heterogeneous models, the outlook for a reliable implementation of the output least squares method would appear dim.

3 The Coherency Method

The hysterical behaviour of the mean-square error function, as described in the last section, is caused by the interaction between the background velocity c_s and the reflectivity r through the definition (2). A possible way out of this dilemma is to decouple c_s and r by treating r, rather than c_r, as the "other" component of the model: thus define

$$\tilde{S}[c_s, r](t,p) = f * \frac{\partial r}{\partial t}(t,p).$$

Certainly if r and c_r are related by (2) then

$$S[c_s, c_r] = \tilde{S}[c_s, r].$$

In fact, apart from the surface normalization, the background velocity c_s enters the definition of $\tilde{S}$ only implicitly, through the condition (2). If we are to use r as one of the independent variables, instead of c_r, we must develop a condition, phrased only in terms of c_s and r, which guarantees that (2) holds. Fortunately, this is rather easy: from the useful perturbational identity

$$\frac{v_r}{v_s^3} \equiv \frac{c_r}{c_s^3} \tag{3}$$

it follows that, if (2) is satisfied, then

$$c_s^{-3}(z)c_r(z) = v_s^{-2}(z,p)r(\tau(z,p),p). \tag{4}$$

The notable quality of (4) is that the left-hand side is independent of p. Thus differentiation with respect to p eliminates c_r altogether:

$$0 = \frac{\partial}{\partial p}[v_s^{-2}(z,p)r(\tau(z,p),p)]. \tag{5}$$

It is easy to reverse this reasoning. Thus:

> *A section $r(t,p)$ is the reflectivity corresponding to a reflection series $c_r(z)$ if and only if (5) is satisfied, in which case c_r is given in terms of $r(t,p)$ and $c_s(z)$ by (4).*

In formulating the constraint given by (5), it is advantageous to return to (t,p) coordinates (the reason will become apparent below). Thus define the quantity $W[c_s,r]$ (the *incoherency*) by

$$W[c_s,r](t,p) = \left\{ \frac{\partial}{\partial p} \left[v_s^{-2}(z,p) r(\tau(z,p),p) \right] \right\} \Big|_{z=\zeta(t,p)} .$$

Then

$$W[c_s,c_r] = S_{data}$$

if and only if

$$\begin{aligned} \tilde{S}[c_s,r] &= S_{data} \\ \text{and} \qquad W[c_s,r] &\equiv 0 \end{aligned}$$

with c_r and r related by (2) and (4).

Of course, the inverse problem is overdetermined, so we replace the exact fit of predicted to measured seismograms by minimization of the mean-square error:

$$\begin{aligned} \min_{c_s,r} \quad & \int\int |\tilde{S}[c_s,r] - S_{data}|^2 dt\, dp \\ \text{subject to} \quad & W[c_s,r] \cong 0 \end{aligned} \tag{6}$$

The constrained least-squares problem (6) has exactly the same solutions as the output-least-squares problem discussed in the preceding section. Since you can't get something for nothing, something must be wrong with (6). The nasty features of (6) are discussed in the companion papers Symes (1988 a,b,c). Essentially (6) does not have the properties which ensure that constrained optimization problems have efficiently computable solutions, depending stably on their data.

To obtain a problem more amenable to numerical solution, we "relax" (6) by making the constraint $W \cong 0$ soft:

$$\min_{c_s,r} \tilde{J}_\sigma[c_s,r,S_{data}] \tag{7}$$

where

$$\tilde{J}_\sigma[c_s,r,S_{data}] = \int\int dp\, dt \left\{ |\tilde{S}[c_s,r] - S_{data}|^2 + \sigma^2 |W[c_s,r]|^2 \right\}$$

We call (7) the *coherency optimization problem.*

From the equivalence above, we see that if S_{data} is *consistent*, i.e. $S_{data} = S[c_s, c_r]$, then the problem (7) has $[c_s, r]$ amongst its solutions for which r and c_r are related by (4). That is, for consistent data, (7) has "the same solutions" as the output least-squares problem (6). We have shown, however, that (7) is far better suited to numerical computation by Newton's method and its relatives, and that the solution of (7) is *stable*, i.e. "degrades gracefully" in the presence of data error, for suitable choices of the penalty parameter σ.

These conclusions hold provided that S_{data} is near (in the mean-square sense) some "exact" or consistent data $S[c_s, c_r]$, and provided that c_s, c_r satisfy certain conditions. "Physical," or poetic, statements of these conditions are:

(i) *c_r should be "rough", i.e. contain significant variation (reflectors), on a length scale dictated both by the wavelet (f) passband and by the smoothness (characteristic length) of c_s;*

(ii) *The range of slownesses p available in the data ("aperture") should be sufficiently large relative to both the degree of roughness mentioned in (i) and the amount of data error, so that the moveout of reflections clearly discriminates the velocities.*

It is easy to see why these conclusions might hold, and at the same time to identify the close link between coherency optimization and *velocity analysis*, as widely practiced in the exploration industry. In fact, to make the first term in the definition of $\tilde{J}_\sigma$ small, i.e.

$$\int\int dp\, dt |\tilde{S}[c_s, r] - S_{data}|^2$$

requires simply deconvolving the data, as is evident from the definition of $\tilde{S}$, given near the beginning of the section. Having removed the influence of the source signature f, the second term

$$\int\int dp\, dt |W[c_s, r]|^2$$

gauges the extent to which c_s reproduces the moveout inherent in the data. In fact, the substitution of $\tau(z, p)$ for t in (5) is a precise ("ray trace")

normal moveout correction; vanishing of the derivative with respect to p detects whether the section is *flat* after the normal moveout correction. Thus minimizing the second term flattens the tau-p reflectivity section in just the way the usual constant-velocity normal-moveout correction flattens events on a CMP section.

The coherency method differs from ordinary velocity analysis in three crucial ways, which are responsible for its feasibility as an automatic velocity estimator. First, since (ray-theoretic) travel time is used to construct the moveout correction, rather than an RMS velocity, the entire tau-p section is flattened, rather than small windows about certain events. Second, the reflectivity section (i.e. part of the *model*) is flattened, rather than data itself. The derivative figuring in the definition of W guarantees that incoherent error in the data will not be fit by r, since such errors would greatly increase the size of W. For the same reason, it is necessary to apply W to the reflectivity model r rather than directly to the data S_{data}. Finally, an obvious alternative measure of flatness after NMO correction is the *semblance*, (a version of) which would be generated by *integrating* in p in equation (5), instead of differentiating, followed by normalization by the RMS power. Such velocity power spectra are commonly used detectors of event-flattening. The most cited reference is Taner and Koehler (1969). These integrated measures of coherence are very robust, so can be applied directly to the data. On the other hand the effectiveness of semblance analysis depends on the nonconvexity of the semblance, i.e. on the sharpness of the peaks, and in fact semblance analysis is essentially equivalent to output-least-squares estimation for a simplified model (Santosa and Symes, (1989), App. A). Therefore, an integrated version of (5) is unsuitable for *automatic* velocity estimation by gradient methods in the same way as is output-least-squares.

The role of conditions (i) and (ii) above is clear from the heuristics of velocity analysis as well. The reflector series c_r, hence each trace in the reflectivity r, must be *rough* or *oscillatory* in the passband of the source signature f in order that the tau-p section contain *events* of significant power. These events must be dense enough and extend over a large enough range of slowness that the moveout constrains the velocity effectively on its characteristic length scale. In effect, the typical event density, seismic velocity range, and cable length determine the resolution limit of velocities. In the next section this resolution limit will be illustrated graphically.

The final change back to travel time in the definition of W is necessary in order that W define a smooth function on appropriate function spaces. Other technical aspects of the coherency method, as well as precise mathematical statements and proofs of our results, may be found in the companion papers Symes [1988a, b, c].

1 Numerical Experiment: Synthetic Data

Implementation of the coherency method in a FORTRAN code (of approximately 3,500 executable lines) involved a large number of choices concerning discretization, approximation, and optimization. A detailed description of the code appears in the technical report (Symes 1988a). For reasons of space, we will describe here only those features which seem to us most important.

First, we repeat the "scan" experiment reported in Section 2, this time displaying the coherency optimization functional

$$\tilde{J}_\sigma[c_s, r, S_{data}] = \int\int dp\, dt \left\{ |\tilde{S}[c_s, r] - S_{data}|^2 + \sigma^2 |W[c_s, r]|^2 \right\} .$$

The integration is over the (tau, p) rectangle displayed in Figure 2, and the integral is discretized using the trapezoidal rule. The various derivatives appearing in the definitions of $\tilde{S}$ and W are approximated by centered differences. The parameter σ is set = 1.

The sampling of $\tilde{J}_\sigma$ over the line in model space (defined in Figures 1, 3) is displayed in Figure 5. The contrast with Figure 4 is dramatic, and provides some evidence that the theoretical convexity results explained in Section 3 are reflected in the actual behaviour of $\tilde{J}_\sigma$.

Next we attempt to recover the model of Figure 1 from the data of Figure 2, by numerical minimization iof $\tilde{J}_\sigma$. This process requires the definition of trial spaces for $c_s(z)$ and $r(t,p)$. For $c_s(z)$ we used a space of exponentiated integrated cubic b-splines:

$$c_s(z) = \exp\left(\int_0^z \sum_{j=2}^{N-2} x_j \psi_j \right)$$

where

$$\psi_j(z) = \Psi\left(N\frac{(z - z_j)}{z}\right), \quad z_j = \frac{j}{N} z_{\max}, \quad j = 0, \ldots N$$

and Ψ is a model cubic b-spline (see DeBoor (1978)). This choice of representation, parameterized by the coefficients x_j, $j = 2, \ldots, N-2$, ensures positivity of the velocity and gives direct control over the amount of smoothness in the model. See Figure 6 for illustration. (Recall that velocities and depths are normalized against the surface velocity.)

For r we used an array of samples:

$$r_{ik} \approx r(i\Delta t, p_k), \quad i = 0, \ldots, nt, \quad k = 1, \ldots, np$$

where $\Delta t = .004$ sec. In principle, the slowness samples p_k are allowed arbitrary spacing. In the synthetics reported in this section, we used 100 equally-spaced slownesses ranging from 0.15 to 0.35. (Recall that slownesses are also normalized against the surface velocity.)

It is inherent in our approach that differentiation of r with respect to t and p must be *bounded* operators, i.e. r derivatives must be measured in such a way as to have essentially the same size as r. This equilibration may be accomplished by using discrete analogues of the *Sobolev norms* to measure the size of r, etc. For details see Symes (1988a).

Correct relative weights must also be established for c_s and r, as these have entirely different units. We have determined the weights up to now by trial and error. An approach like that described by Kennett *et al.* (1988) may circumvent this difficulty, and is under study.

We coupled subroutines for $\tilde{J}_\sigma$ and its derivatives with respect to the velocity parameters x_j and the reflectivity parameters r_{ik} to an optimization routine of *truncated Gauss-Newton* type, described in Santosa and Symes (1989, Ch. 10). This algorithm *interpolates* between steepest descent iteration and the Gauss-Newton iteration in a controllable way. In general, steepest descent iteration is more reliable far from a minimum, whereas Gauss-Newton iteration is more rapidly convergent near a solution (see e.g. Dennis and Schnabel (1983)). Our algorithm in effect switches continuously between the two, and achieves assured convergence to a local minimizer with some efficiency, at least in principle.

Other reasonable choices of optimizer are certainly possible. We regard the optimal choice of strategy as open, at present, partly for the reasons to be discussed below.

The velocity function in Figure 1 belongs to the model space described above with $N = 16$, $z_{\max} = 1.25$ sec. We applied the algorithm just described to the data of Figure 2, and after 10 Gauss-Newton steps achieved the estimate of c_s depicted in Figure 7. The initial estimate of c_s was $c_s(z) \equiv 1$. Rather than display the resulting reflectivity, we give the *stack*

$$\frac{c_s^3(z)}{|p_{\max} - p_{\min}|} \int_{p_{\min}}^{p_{\max}} dp\, v_s^{-2}(z,p) r(\tau(z,p),p)$$

which should reproduce c_r if r is exactly correct. As Figure 8 shows, the major features of c_r are recovered, but with some loss of energy. This inaccuracy occurs at least in part because of the relative-scale problem mentioned above. The estimate for r can be "cleaned up" somewhat by holding c_s fixed at Figure 7 and taking a number of additional steps in r alone. The stack resulting from this process is displayed in Figure 9.

Another gauge of the extent to which the inversion is successful is eyeball assessment of the extent to which the NMO correction for the estimated velocity function *flattens* the estimated reflectivity section. In Figure 10 we display the NMO-corrected before-stack reflectivity

$$c_s^3(z) v_s^{-2}(z,p) r(\tau(z,p),p)$$

and in Figure 11 the same using the exact c_s and r.

A crude measure of the roboustness of this process is its sensitivity to additive noise in the data section S_{data}. We added 50% RMS relative pseudo random noise, filtered by the source wavelet, to the data of Figure 2; the result is given in Figure 12. The estimated velocity and reflectivity appear in Figures 13 and 14. Note the role of the coherency constraint in keeping the reflectivity "clean": any incoherent noise drastically increases W, and is therefore not modeled. In effect, coherency optimization implements a moveout-adapted dip filter.

5 Numerical Experiments: Field Data

To make a preliminary assessment of the practicality of the method described in the preceding paragraphs, we applied it to a tau-p data set produced from a marine survey conducted in the Gulf of Mexico.

The survey consisted of 511 shot profiles (shot interval 22.5 meters) collected with a streamer containing 301 hydrophone groups. The group interval was 15 meters with a minimum separation of 148 meters. Each group contained 17 equally spaced and equally weighted phones. The data were recorded without a low-cut filter; a 110 Hz. high-cut filter was applied; the sampling rate was .002 sec.; total record length was 5 sec. A portion of a 50-fold near-trace common midpoint stack is shown in Fig. 13. This area of the Gulf contains a strong gas-sand related direct hydrocarbon indicator (DHI) located near 2.3 sec.; it is readily apparent in the stack.

The data were prepared by carrying out shot-gather based wavelet estimation and deconvolution designed to remove a mild low- frequency linear noise observed in the data. An isotropic two-lobed minimum phase gaussian wavelet was employed. The data were sorted to midpoint order, merged into bins containing up to 301 offsets, interpolated to a uniform spacing of 7.5 meters and radially slant stacked. The antenna pattern of the receiver array was computed and compensated to produce a true plane-wave decomposition. The 250 computed plane wave slownesses correspond to an angular range of 11 to 70 degrees at the streamer.

The result is shown in Fig. 14. Inspection of Fig. 14 shows a rich sequence of apparently primary reflections, culminating at approximately 2.3 sec. in the DHI event mentioned above. Below the DHI, the character of the data changes markedly, to a regime of slower events, presumably multiple reflections.

An additional source estimation process was carried out after the plane-wave decompostion. Both wavelet shape and directivity were re-estimated. A line average of the water-bottom reflection event was computed and the result fit to the wave equation prediction for P-wave reflection at a fluid-solid interface. The resulting p-dependent estimated source wavelet was used in the inversion.

Finally the tau-p gather of Fig. 14 was subjected to a deghosting filter and a further tapered 50 Hz. high-cut filter, resampled to .004 sec., and windowed to 100 traces of duration 2.5 sec. The resulting gather, shown in Fig. 15, was the input data set for the inversion.

Application of the damped Gauss-Newton algorithm produced the velocity estimates depicted in Fig. 16. These are displayed alongside a velocity profile extracted from a sonic log taken from a well near the midpoint in question.

The first of several difficulties in assessing these results is evident in Fig. 16. The estimated velocity compares quite well with the log velocity trend, where both are available. Since the log only covers a segment of the well (in this case approximately 1400 - 2500 meters depth), however, the full depth range of the velocity estimate cannot be compared.

Another index of successful velocity estimation is the extent to which NMO correction flattens the reflectivity gather. The NMO-corrected estimated reflectivity gather is displayed in Fig. 17. Several features of this gather deserve comment. First, the lateral continuity of events is considerably enhanced relative to that displayed in the data gather (Fig. 15). This moveout- adapted dip filter effect was noted in the previous section. Most of the moveout has indeed been removed. Some residual moveout remains, however; apparently the reflectivity is slightly overcorrected at the shallower depths and undercorrected at the DHI. We speculate that this effect is partly due to the peculiar structure of the DHI: careful inspection of the data shows that this event undergoes a phase shift at about trace 60, and another at about trace 85. We are unsure as to the cause of these phase anomalies, which are present in neighboring midpoints as well. Obvious possibilities are elastic reflection effects and thin-bed tuning. In any case, the dip filter effect of our optimization turned the phase shift into moveout, which forced overcorrection of overlying events.

Since we used a globally precritical gather with a fixed range of slowness for all times (i. e. a rectangular mute pattern) the range of angles available to constrain the shallow part of the velocity is quite small. We expect that a mute pattern better adapted to the velocity structure, employing different slowness ranges at different depths to keep the angular aperture as constant as possible, would better constrain the shallower velocities and prevent this

overcompensation for deeper non-primary-acoustic artifacts, to some extent. Such a mute pattern could be estimated adaptively; we hope to implement adaptive mute estimation in a future version of the code.

It is also known from logging that the density fluctuates considerably throughout this region. The general acoustic reflectivity varies systematically with slowness in a different way than the constant-density reflectivity. We have verified in subsequent numerical experiments that neglect of this difference can cause systematic misestimation of velocity, through the amplitude dependence of the incoherency operator W. Since our current code is based on the constant-density assumption, some of the inaccuracy of the velocity estimate might be due to actual density fluctuations in the real earth. This is an obvious matter for further study.

The identities and depths of events also diagnose the success of an inversion. In the present approach these are estimated by the stacked reflection series estimate, which is also displayed alongside the log in Fig. 16 (bottom curve). The DHI is easily identifiable, as is the event near 1520 meters Both are placed about 80 meters too deep, consistent with the slightly high velocity estimate in the logged zone and the overcorrection of shallow events noted above.

In summary, this preliminary test achieved a modest degree of success: a reasonable velocity model, accounting for the bulk of the moveout in the data, was estimated entirely automatically. Several causes for the residual inaccuracies, consistent with the layered medium hypothesis, suggested themselves, and remedies will be pursued in subsequent work.

6 Coherency Optimization for Laterally Heterogeneous Models

The essential ingredients of the approach to velocity inversion sketched in the previous section were:

(i) parameterization of the reflectivities as time "sections" (i.e. traces), so that the seismogram is a regular function of the reflectivities, one reflectivity (trace) per plane-wave "shot" (synthetic source);

(ii) referral of each time-section reflectivity to depth, and assessment of the dependence of the resulting suite of depth sections on the "shot" parameter (i.e. slowness).

In this section, we maintain the fiction that the seismogram is adequately approximated by the multi-dimensional version of the convolutional model, i.e., the linearization about a smooth background velocity, and moreover apply high-frequency asymptotics freely. A natural interpretation of (i) and (ii) emerges in this context.

First recall *why* the parameterization by two-way time resulted in regularity of the seismogram as a function of *both* the background velocity and the reflectivity. In effect, each reflector was associated with the time of arrival, at the surface, of its reflection. If the background velocity is changed, then depth-parameterized reflectors remain fixed while their reflection times change, whereas time-parameterized reflectors remain fixed while their depths change. In the former case, high-frequency arrivals are time-shifted, while in the latter case they are not. The time-shift is a time *derivative* in the infinitesimal limit, and its appearance marks the loss of regularity of the depth-parameterized reflectivity-to-travel-time map. For time-parameterized reflectivities, no such time shift occurs as a result of background velocity change, and regularity is maintained.

Reflectors and reflection arrivals are both (near)-singularities, i.e. locii of high-frequency energy. In the high-frequency limit, therefore, we must ask: how can we parameterize reflectivity so that a singularity in the reparameterized reflectivity corresponds, under conversion to ordinary spatial coordinates and mapping to the seismogram, to a singularity in the same location? In several-dimensional problems, singularities may have *orientations*, and these must be preserved as well.

This question is answered by a theorem of Rakesh (Symes (1985), Rakesh (1988)), together with a construction presented for this problem by Beylkin (1985). To fix ideas, suppose we consider the linearized acoustic problem for a point source, which models a shot-gather:

$$\frac{1}{c_s^2}\frac{\partial^2 u}{\partial t^2} - \nabla^2 u = \frac{2r_z}{c_s^2}\frac{\partial^2 u_0}{\partial t^2}$$

where $r_z = c_r/c_s$ is the "reflectivity depth section", c_s is the background velocity, u is the scattered field, and u_0 is the reference field satisfying

$$\frac{1}{c_s^2}\frac{\partial^2 u_0}{\partial t^2} - \nabla^2 u_0 = f(t)\delta(\underline{x} - \underline{x}_s),$$

$\underline{x}_s$ being the source location. Rakesh showed that for the impulsive case ($f(t) = \delta(t)$) a singularity in r_z at the subsurface location $\underline{y}$, across a surface element with normal $\underline{\eta}$, corresponds to a singularity in the reflected field at receiver location $\underline{x}_r$, time t_r, only if there exist

- an incident ray γ_i associated with the reference field, emanating from the source-point $\underline{x}_s$ at $t = 0$;
- a reflected ray γ_r, passing over the receiver point $\underline{x}_r$ at time t_r

so that γ_i and γ_r meet at the reflector point $\underline{y}$ at some intermediate time, making equal-angles with the reflector normal $\underline{\eta}$. For non-impulsive but broad-band time signatures $f(t)$, this rule governs the arrival of (primary-reflected) high-frequency energy.

This is exactly the usual picture of the reflection process, of course. Rakesh's theorem, which justifies this picture in terms of the wave equation, holds in complete generality, so long as the background velocity c is smooth. It tells us exactly which singularity in the time section must be mapped to a given singularity in the depth section if the seismogram is to return such singularities to their original position and orientation. Beylkin's construction, on the other hand, applies only when no *caustics* exist in the incident field, i.e. each depth point $\underline{y}$ is joined to the source point $\underline{x}_s$ by a unique incident ray. Then *any* mapping having the singularity-moving properties just described must differ only by a (possibly frequency-dependent) amplitude modulation (technically, a pseudodifferential operator) from the Kirchhoff migration formula

$$\begin{aligned} r_z(\underline{y}, \underline{x}_s) &= Kr(\underline{y}, \underline{x}_s) \\ &= \int d\underline{x}_r \, w(\underline{x}_s, \underline{y}, \underline{x}_r) r(\underline{x}_r, \tau(\underline{x}_s, \underline{y}, \underline{x}_r), \underline{x}_s). \end{aligned} \tag{8}$$

Here $\tau(\underline{x}_s, \underline{y}, \underline{x}_r)$ is the two-way reflection phase, i.e. the time from $\underline{x}_s$ to $\underline{y}$ to $\underline{x}_r$, and $w(\underline{x}_r, \underline{y}, \underline{x}_s)$ is a slowly-varying amplitude modulation.

Thus: the reflectivity time-sections $r(\underline{x}_r, t, \underline{x}_s)$ will be converted to reflectivity depth sections $r_z(\underline{y}, \underline{x}_s)$ via a Kirchhoff migration formula like (8). This relation implicitly defines the seismogram as a function of $r(\underline{x}_r, t, \underline{x}_s)$, and guarantees that it is regular as a function of c_s, r. Note the apparent similarity of (8) to the travel-time change-of-variables, appropriate in the layered case (formula (A.1), for instance).

The second ingredient (ii) in the coherency optimization approach is evidently the condition that the depth-parameterized reflectivities $r_z(\underline{y}, \underline{x}_s)$ are actually independent of $\underline{x}_s$ ("Every shot sees the same earth"). Regarding the source locations as filling up a continuum, this amounts to the condition $\nabla_{\underline{x}_s} r_z(\underline{y}, \underline{x}_s) = 0$. The composition rules for oscillatory integrals (the local calculus of Fourier Integral operators—e.g. Duistermaat (1973), Ch. 2) give the result:

$$\nabla_{\underline{x}_s} r_z = \nabla_{\underline{x}_s} K r = K(\nabla_{\underline{x}_s} + P) r$$

up to an error rapidly decaying in frequency content, where P is a *pseudodifferential operator* in $\underline{x}_r$ and t, i.e. an oscillatory integral of the form

$$Pr(\underline{x}_r, t) = \int\int d\underline{x}\, ds\, d\underline{k}\, d\omega\, e^{i[\underline{k}\cdot(\underline{x}_r - \underline{x}) + \omega(t-s)]} p(\underline{x}_r, t, \underline{x}_s, \underline{k}, \omega) r(\underline{x}, s).$$

The amplitude p depends on the ray geometry, i.e. on the background velocity c_s, but the phase $\underline{k}(\underline{x}_r - \underline{x}) + \omega(t-s)$ does not. Thus $(\nabla_{\underline{x}_s} + P)r$ is regular as a function of c_s, i.e. perturbing c_s does not result in the appearance of higher derivatives of r, just as was the case for the formula (A.1) for $W[c_s, r]$.

Now let L be any operator from depth-parameterized reflectivities to sections which has the reverse effect to K on singularities: for instance L might be taken as the linearized seismogram operator itself. Then another application of the same reasoning shows that

$$W[c_s, r] := L \nabla_{\underline{x}_s} K r$$

is regular as a function of c_s, r for the same reason. We take this formula as our definition of the incoherency for the laterally heterogeneous acoustic problem. Note that L must be computed to form the seismogram, and K is the Kirchhoff migration operator (or an equivalent). Thus $W[c_s, r]$ involves only well-understood computations.

The attentive reader will note the immediate resemblance to the definition of $W[c_s, r]$ given in Section 2.

Thus the transformation $\tilde{r} \rightarrow Kr$ serves the role of the travel-time transformation. The special role of travel-time in regularizing 1-d problems was noted in the work of Gray (1980). Some time later, Gray and Hagin (1984) attempted generalized travel-time coordinates for laterally heterogeneous point source problems, with limited success; travel-time (ray-straightening) coordinates *per se* do not exist in general for several-dimensional problems. Nonetheless, the operator K accomplishes the principal effect of the 1-d travel-time coordinate, i.e. to make reflector location independent of background velocity in both the (reparameterized) reflectivity and in the seismogram simultaneously. Of course, K is a more complicated operator than a change of coordinates, except for 1-d (plane-wave, layered model) problems.

The very close relation of the method described here to "migration velocity analysis" (e.g. Al-Yahya (1989)) is also clear. In fact $W[c_s, r]$ vanishes exactly when the migrated gathers Kr are flat — in fact all traces are equal — with respect to shot parameter, i.e. "when sorted to receiver gathers." The differences between the two approaches are exactly parallel to the differences between the layered coherency method and standard NMO-velocity analysis, as described at the end of Section 3. Specifically, the method described here is based on a *differential* measure of coherence, applied to the *model*, whereas migration velocity analysis is based on an integral measure (analogous to semblance) applied to (migrated) data.

We conclude that both main ingredients of coherency optimization, as explained in Section 2 for layered acoustics, generalize in an acceptable way to a simple laterally heterogeneous model. Many details remain to be settled, some of which will doubtless be crucial to computational efficiency. Also, the analysis cited in Section 3 remains to be generalized. A technical complication is that, while the operators L and K exist in general, the composition rules leading to the regularity of the incoherency $W[c_s, r]$ must be modified when caustics are present. Nonetheless, we have established that the coherency approach is not restricted conceptually to layered problems.

1 Discussion and Conclusion

1.1 The scope of the coherency approach

From a theoretical point of view, and perhaps from a practical one as well, the chief defect in the results of the preceding sections on the layered acoustic problem is the absolute lack of any provision for multiple reflections. This defect is cured in the companion paper Symes [1988c], in which the fully nonlinear bandlimited layered velocity inversion problem is treated with full mathematical rigor. We reach a qualitatively identical conclusion about the appropriate version of coherency optimization: that is, it gives a (regularized) solution of the inverse problem stably dependent on near-consistent data, provided that sufficiently many reflectors are present, i.e. that the target profile is sufficiently *rough*. We give a precise sense for "rough", and a relation emerges between stability, aperture, bandlimits, and roughness (reflector density) very similar to that explained in Section 3.

Both convolutional model and fully nonlinear versions of other layered inverse problems should succumb to the same approach. We mention specifically nonconstant-density acoustics, the "marine" elastic model (with sources and receivers in an overlying fluid layer), and either of these with the source time-dependence and directivity also regarded as unknowns. Some idea of the novel features of these problems in convolutional approximation may be gleaned from Sacks and Symes (1987) and Bube, Lailly, Sacks, Santosa, and Symes (1989). No technical obstacles appear to lie in the way of an analogous treatment of these problems.

Note that the density, regarded as independent of velocities, will not be recovered with trend, in any of these problems, as density trend perturbations do not affect ray geometry. This gross density ambiguity is well-known (Tarantola (1986)) and has been observed in output-least-squares results (Canadas and Kolb, (1986)).

The program outlined in Section 6 appears feasible. On the other hand, while an analogous coherency optimization principle can be formulated for fully nonlinear laterally heterogeneous models, its analysis will require fundamental advances in the understanding of wave propagation in rough media.

7.2 Conclusion

We have presented a novel approach to the reflection seismic inverse problem, which has its roots in utterly commonplace concepts in seismic data processing. We have formulated this coherency optimization principle precisely for the convolutional approximation to the layered constant-density acoustic model. We displayed the results of numerical experiments with both simulated and field plane-wave data sets. The results of these experiments suggest that the method is "practical," and that it produces reasonably accurate and stable estimates of both velocity trends and reflectivities, to the extent that these are determined by the precritical plane-wave data set used. In particular, the coherency method extracts reasonable velocity estimates in cases in which output least squares inversion fails completely, viz. when the trend of the initial velocity estimate is grossly incorrect. Finally, we formulated an analogous principle for laterally heterogeneous velocity inversion, a problem for which output-least-squares inversion is so inefficient as to be infeasible. It remains to be seen whether coherency optimization yields a computationally tractable approach to such several-dimensional problems.

References.

AL YAHYA, K.M. [1989]. Velocity Analysis by iterative profile migration, *Geophysics 54*, pp. 718-729.

BAMBERGER, A., G. CHAVENT, C. HEMON, and P. LAILLY [1982]. Inversion of normal incidence seismograms, *Geophysics 47*, pp. 757-770.

BEYLKIN, G. [1985]. Imaging of discontinuities in the inverse scattering problem by inversion of a causal generalized Radon transform, *J. Math. Phys. 26*, pp. 99-108.

BRYSK, H. and D. MCCOWAN [1986]. A slant-stack procedure for point-source data, *Geophysics 51*, pp. 1370-1386.

BUBE, K., P. LAILLY, P. SACKS, F. SANTOSA, and W. SYMES [1989]. Simultaneous determination of source wavelet and velocity profile using impulsive point-source data from a layered fluid, *Geophys. J. Roy. Astr. Soc. 95*, pp. 449-462.

BUBE, K., D.B. JOVANOVICH, R.T. KANGAN, J.R. RESNICK, R.T. SHUEY, and D.A. SPINDLER [1985]. Well-determined and poorly determined features in seismic reflection tomography: Part II, 55th Annual Meeting, SEG, Washington, DC.

BEYLKIN, G. and R. BURRIDGE [1987]. Linearized inverse scattering problems of acoustics and elasticity, preprint; also Multiparameter inversion for acoustic and elastic media, Expanded Abstract, 57th Annual International Meeting, Society of Exploration Geophysicists, New Orleans, pp. 747-749.

CANADAS, G. and P. KOLB [1986] Least-squares inversion of prestack data: simultaneous identification of density and velocity of stratified media, Expanded abstract, 56th Annual International Meeting, Society of Exploration Geophysicists, Houston, pp. 604-607.

CAO, D., W. BEYDOUN, S. SINGH, and A. TARANTOLA [1989]. Simultaneous inversion for background velocity and impedance maps, I. P. G. Preprint.

CLAYTON, R. and R. STOLT [1981]. A Born-WKBJ inversion method for acoustic reflection data, *Geophysics, 46*, pp. 1559-1567.

COHEN, J.K. and N. BLEISTEIN [1979]. Velocity inversion procedure for acoustic waves, *Geophysics 44*, pp. 1077-1085.

DENNIS, J. E. JR. and R. B. SCHNABEL [1983]. *Numerical Methods for Unconstrained Optimization and Nonlinear Equations*, Prentice-Hall, Englewood Cliffs.

DUISTERMAAT, J. [1973]. Fourier Integral Operators, Courant Institute Lecture Notes.

GAUTHIER, O., TARANTOLA, A. and VIRIEUX, J. [1986]. Two-dimensional nonlinear inversion of seismic waveforms, *Geophysics 51*, pp. 1387-1403.

GRAY, S.H. [1980]. A second-order procedure for one-dimensional velocity inversion, *SIAM J. Appl. Math. 39*, pp. 456-462.

GRAY, S. and F. HAGIN [1984]. Travel-time-like variables and the solution of velocity inverse problems, preprint.

HADJEE, Y. and F. COLLINO [1988]. A geometrical approach to the a-priori study of the 1-d inverse problem, IFP preprint.

IKELLE, L. , J. DIET and A. TARANTOLA [1988]. Linearized inversion of multioffset seismic data in the omega-k domain: depth-dependent reference medium, *Geophysics 53*, pp. 50-64.

KENNETT, B. L. N., M. S. SAMBRIDGE, and P. R. WILLIAMSON [1988]. Subspace methods for large inverse problems with multiple parameter classes, *Geophys. J. 94*, pp. 237-247.

KOLB P., F. COLLINO, and P. LAILLY [1986]. Prestack inversion of a 1D medium, *Proc. IEEE 74*, pp.498-506.

LINES, L. and S. TREITEL [1984]. A review of least-squares inversion and its application to geophysical problems, *Geophysical Prospecting 32*, pp. 159-186.

LINES, L., A. GERSZTENKORN, J. SCALES and S. TREITEL [1987] Fast lp solution of large, sparse linear systems: Application to seismic traveltime tomography, *Geophys. J. Roy. Astr. Soc. 90*, p. 285.

LINES, L., A. SCHULTZ and S. TREITEL [1988]. Cooperative inversion of geophysical data, *Geophysics 53*, pp. 8-20.

MCAULAY [1985]. Prestack inversion with plane-layer point source modeling, *Geophysics 50*, pp. 77-89.

MCAULAY, A. [1986]. Plane-layer point-source prestack inversion of marine data with unknown initial profile, Expanded Abstract, 56th Annual Meeting of the Society of Exploration Geophysicists, Houston, pp. 537-539.

MORA, P. [1986]. Nonlinear 2-d elastic inversion of multi-offset seismic data, Expanded abstract, 56th Annual International Meeting, Society of Exploration Geophysicists, Houston, pp. 533-537; also *Geophysics 52*.

MORA, P. [1987]. Nonlinear 2-d elastic inversion of real data, Expanded abstract, 57th Annual International Meeting, Society of Exploration Geophysicists, New Orleans, pp. 430-432.

PAN, G. S., R. A. PHINNEY and R. I. ODOM [1988]. Full-waveform inversion of plane-wave seismograms in stratified acoustic media: Theory and feasibility, *Geophysics 53*, pp. 21-31.

PAN, G. S. and R. A. PHINNEY [1989]. Full-waveform inversion of plane-wave seismograms in stratified acoustic media: Applicability and limitations, *Geophysics 54*, pp. 568-580.

RAKESH [1988]. A linearized inverse problem for the wave equation, *Comm. on P. D. E. 13*, pp. 573-601.

SACKS, P. and W. SYMES [1987]. Recovery of the elastic parameters of a layered half-space, *Geophys. J. Roy. Astr. Soc. 88*, pp. 593-620.

SANTOSA, F. and W. SYMES [1988]. High frequency perturbational analysis for the point-source response of a layered acoustic medium, *J. Comp. Phys. 74*, pp. 318-381.

SANTOSA, F. and W. SYMES [1989]. *An analysis of least-squares velocity inversion*, Society of Exploration Geophysicists, Geophysical Monograph Number 4, Tulsa.

SANTOSA, F. and W. SYMES [1988]. High frequency perturbational analysis for the point-source response of a layered acoustic medium, *J. Comp. Phys. 74*, pp. 318-381.

SPRATT, S. [1987]. Effect of normal moveout errors on amplitude versus offset-derived shear reflectivity, Expanded Abstract, 57th Annual International Meeting, Society of Exploration Geophysicists, New Orleans, pp.634-637.

SYMES, W. [1985]. Stability and instability results for inverse problems in several-dimensional wave propagation, *Proc. of Seventh Internat. Conf. on Computing Methods in Applied Science and Engineering* (INRIA).

SYMES, W. [1988a]. Velocity Inversion by Coherency Optimization, Rice University, Department of Mathematical Sciences Technical Report 88-4.

SYMES, W. [1988b]. Velocity inversion: a case study in infinite-dimensional optimization, Rice University, Department of Mathematical Sciences Technical Report 88-14 (to appear in *Math. Programming*).

SYMES, W. [1988c]. Bandlimited Velocity inversion: a model inverse problem from reflection seismology, Rice University, Department of Mathematical Sciences Technical Report 88-13.

TANER, M. T. and F. KOEHLER [1969]. Velocity spectra: digital computer derivation and application of velocity functions, *Geophysics 34*, pp. 859-881.

TARANTOLA, A. [1984]. The seismic reflection inverse problem, in *Inverse Problems of Acoustic and Elastic Waves*, ed. Santosa et al., SIAM, Philadelphia.

TARANTOLA, A. [1986]. A strategy for nonlinear elastic inversion of seismic reflection data, *Geophysics 51*, pp.1893-1903.

TREITEL, S., P. R. GUTOWSKI, and D. E. WAGNER [1982]. Plane-wave decomposition of seismograms, *Geophysics 47*, pp. 1375-1401.

Captions

1. Background velocity and reflector series for synthetic examples.

2. Convolutional plane-wave seismogram corresponding to the model of Fig. 1.

   - One-way time interval: 0 – 1.5 sec.
   - Normalized slowness range: 0.15 – 0.35.
   - Source: Ricker wavelet peaked at 20 Hz., isotropic radiation pattern.

3. Velocity trend perturbation.

4. Scan of mean-square error over line segment connecting constant background velocity with that displayed in Fig. 1.

5. Scan of incoherency W over the same segment of velocity models as used to produce Fig. 4.

6. a. Cubic b-splines.

   b. Integrated cubic b-splines.

7. a. Estimated velocity. 10 Gauss/Newton/trust region steps; constant initial velocity, zero initial reflectivity. Shown are the target (solid line) and iterates 1, 2, 3, and 10. Note that the general trend is achieved in three steps.

   b. Velocity components of gradient at iterations 1, 2, 3, and 10.

8. The black line is the target reflection series (Figure 1). The red line is:

   a. stack from reflectivity estimate after 10 Gauss/Newton steps.

   b. stack from reflectivity estimate after 30 additional conjugate residual steps, holding the velocity estimate fixed at the result displayed in Fig. 7.

9. NMO-corrected final reflectivity estimate.

10. Data with 50% RMS pseudorandom passband noise.

11. a. Black line: target velocity model (Figure 1).
    b. Red line: velocity estimate, 0% data noice (Figure 7), 10 Gauss/Newton steps.
    c. Grey line: velocity estimate from data in Fig. 10, 10 Gauss/Newton steps.
12. Final reflectivity estimate corresponding to Fig. 11.
13. Gulf of Mexico data: CDP stack.
14. Gulf of Mexico data: Plane wave decomposition of a midpoint gather.
15. Gulf of Mexico data: windowed, deghosted, filtered, and resampled version of Figure 14. Input data for inversion.
16. Results of inversion: top curves are velocity estimate (smooth curve) and interpreted sonic log (ragged curve). Bottom curve is stacked reflection series estimate. Products of 10 Gauss-Newton steps.
17. NMO corrected reflectivity corresponding to results of Fig. 16.

FIGURE 1

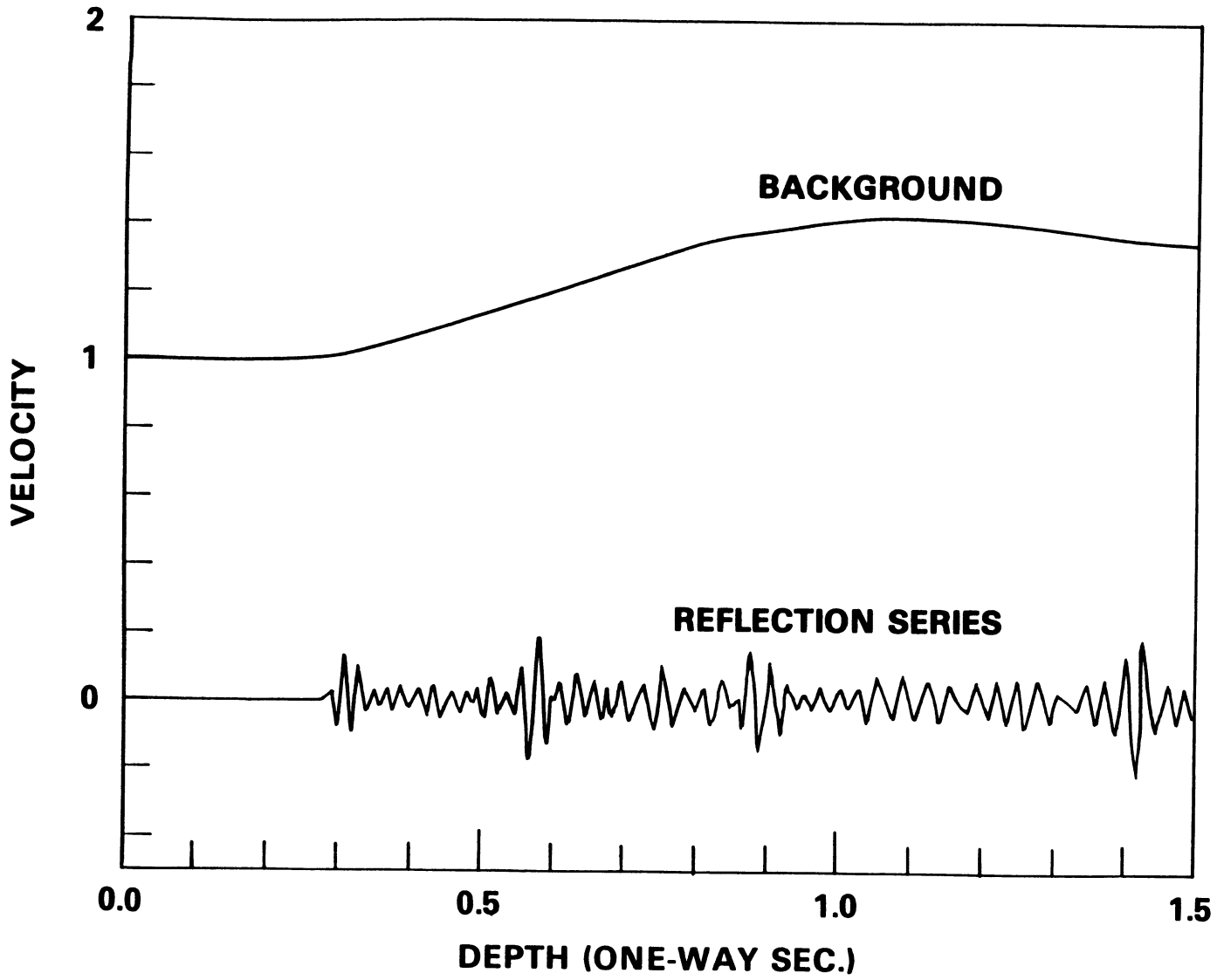
2
1
0
VELOCITY
BACKGROUND
REFLECTION SERIES
0.0
0.5
1.0
1.5
DEPTH (ONE-WAY SEC.)

FIGURE 2

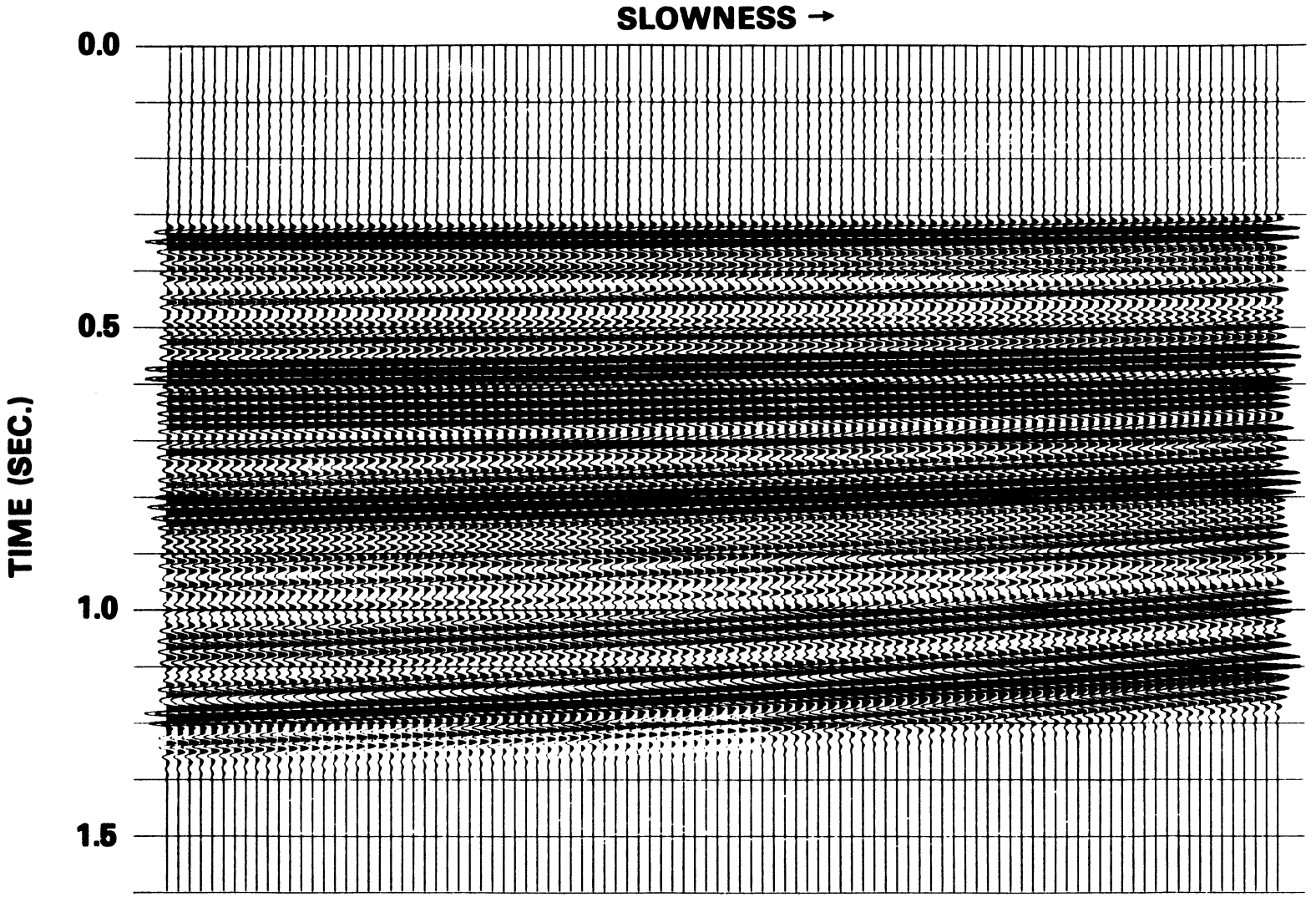

FIGURE 3

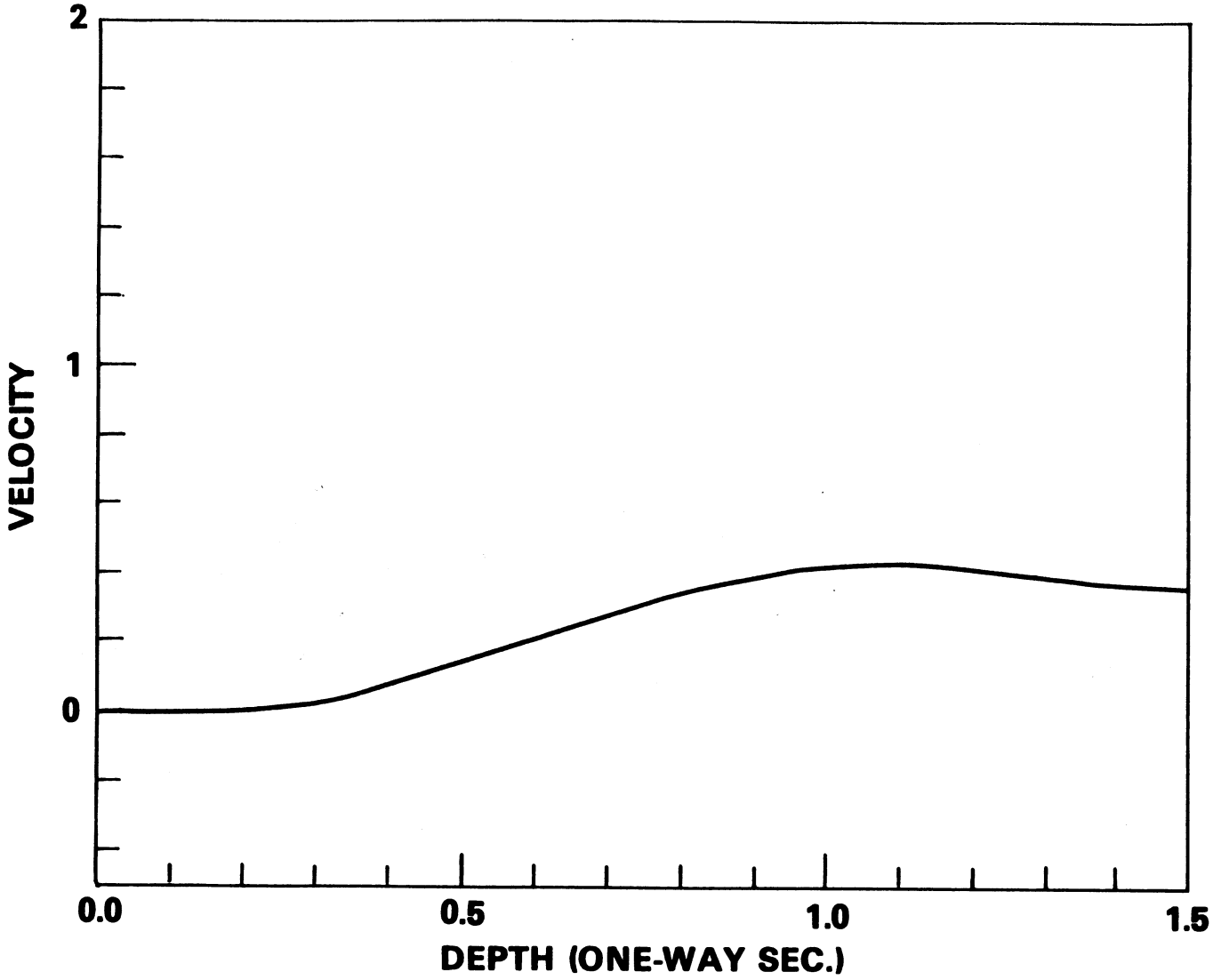

FIGURE 4

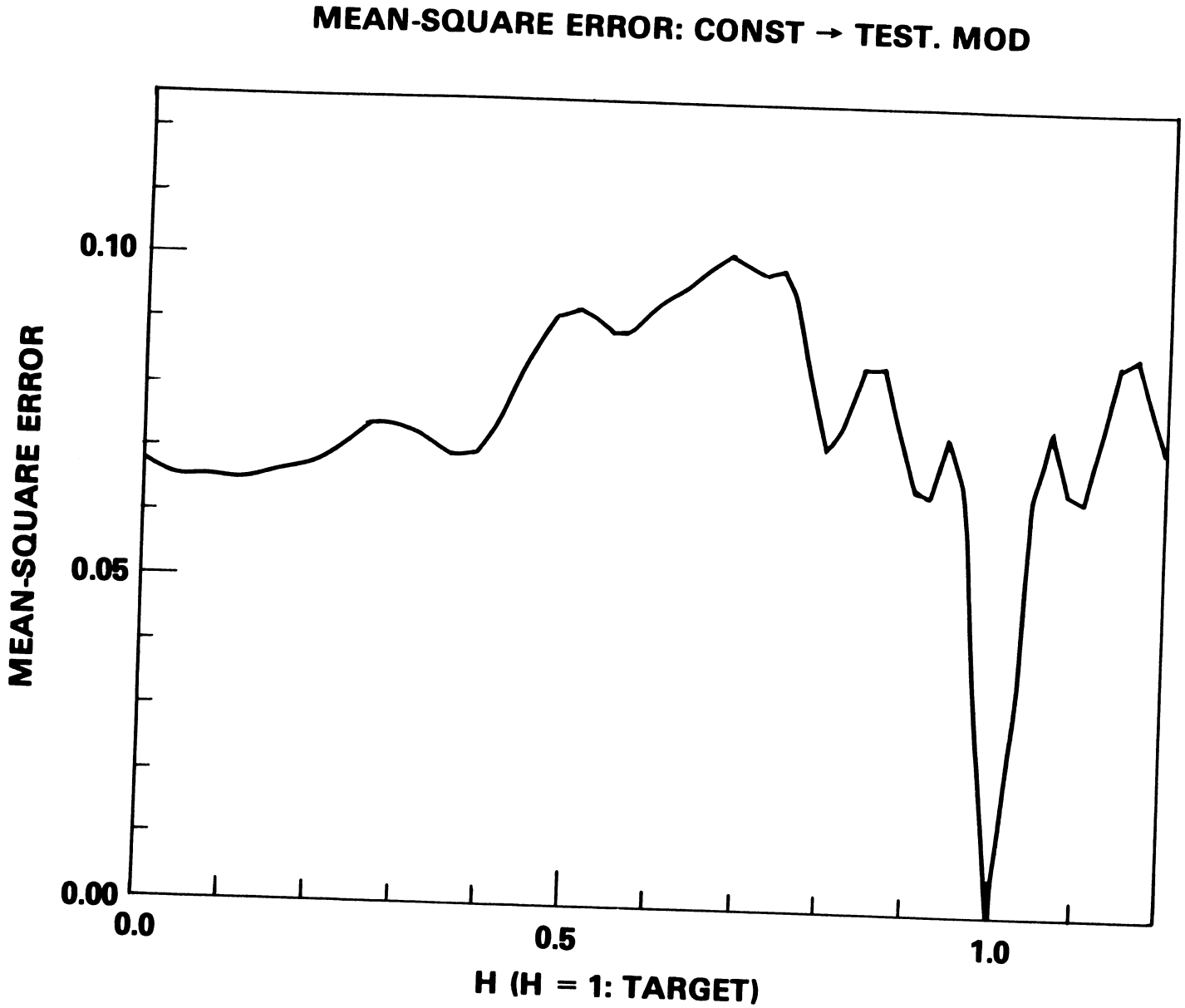
MEAN-SQUARE ERROR: CONST → TEST. MOD
MEAN-SQUARE ERROR
0.10
0.05
0.00
0.0
0.5
1.0
H (H = 1: TARGET)

FIGURE 5

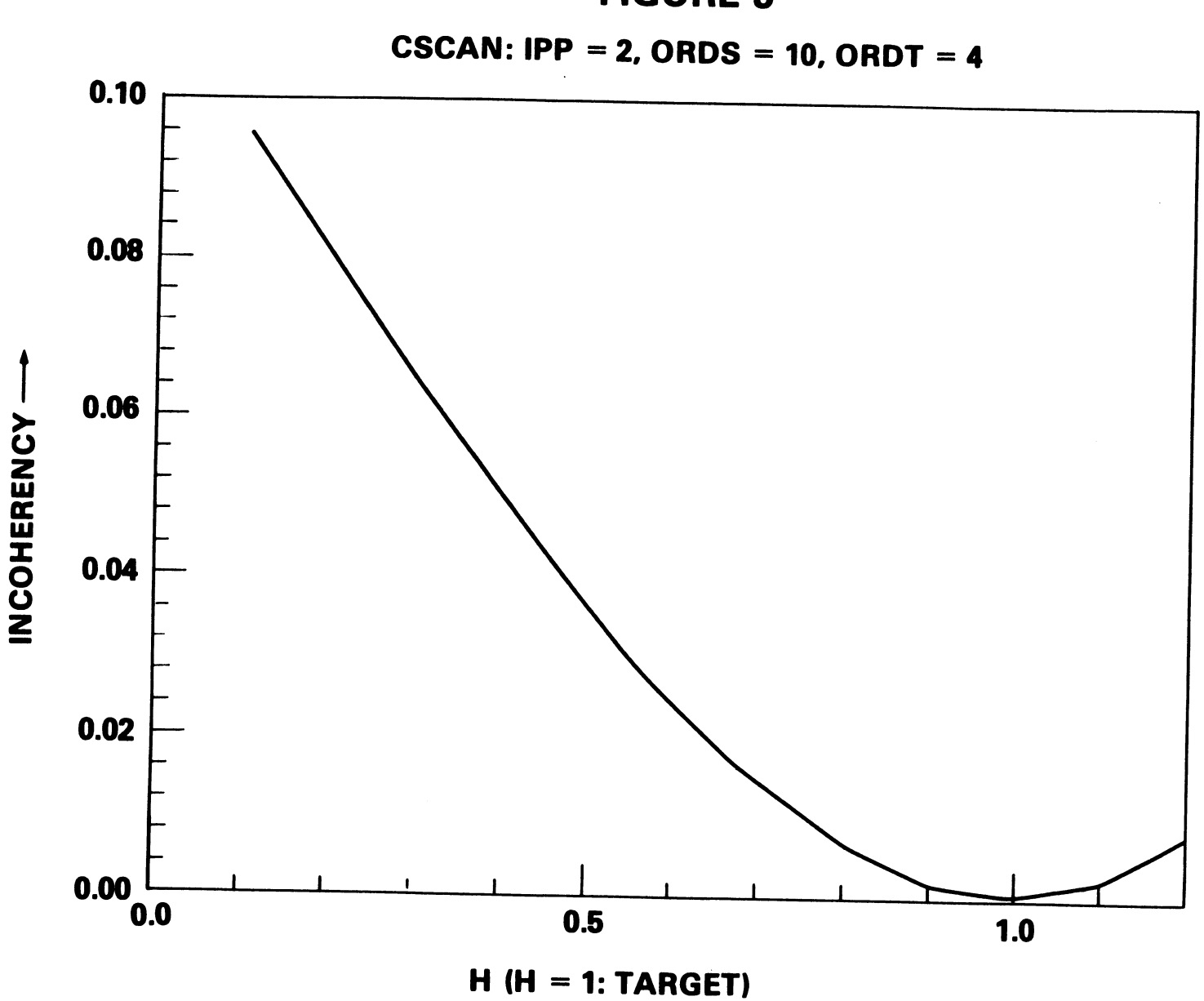
CSCAN: IPP = 2, ORDS = 10, ORDT = 4
0.10
0.08
0.06
0.04
0.02
0.00
INCOHERENCY
0.0
0.5
1.0
H (H = 1: TARGET)

FIGURE 6A

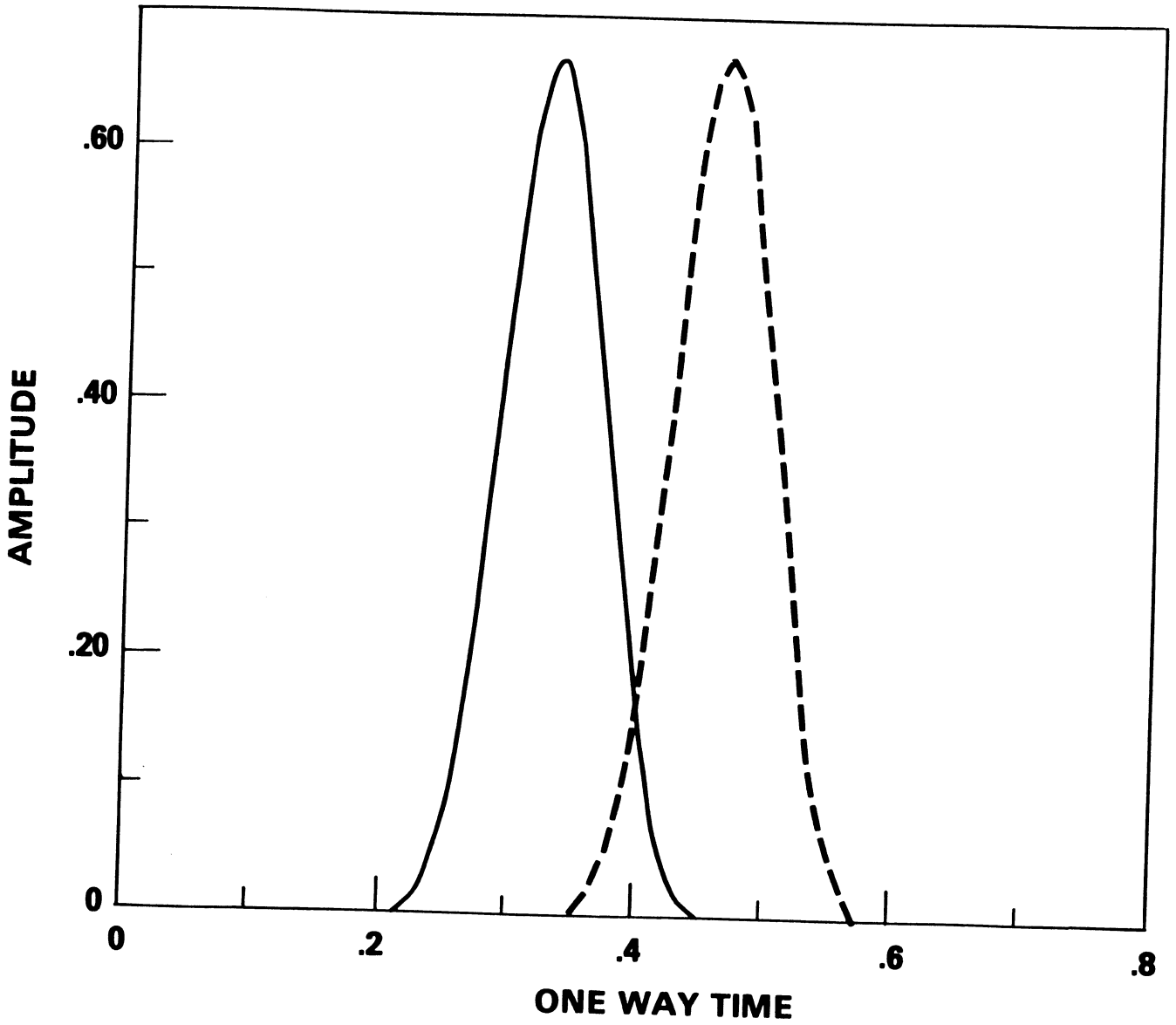

FIGURE 6B

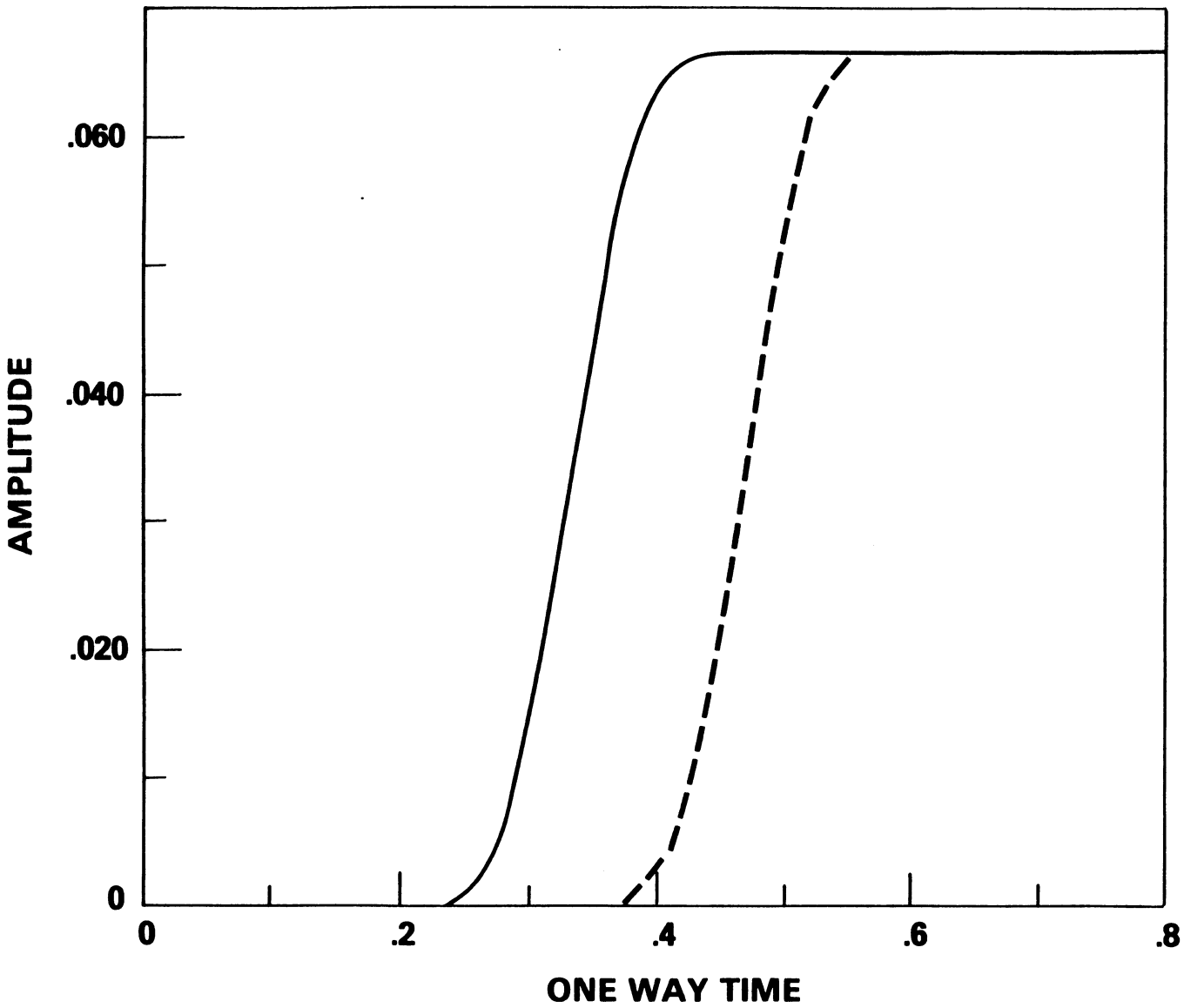

FIGURE 7A

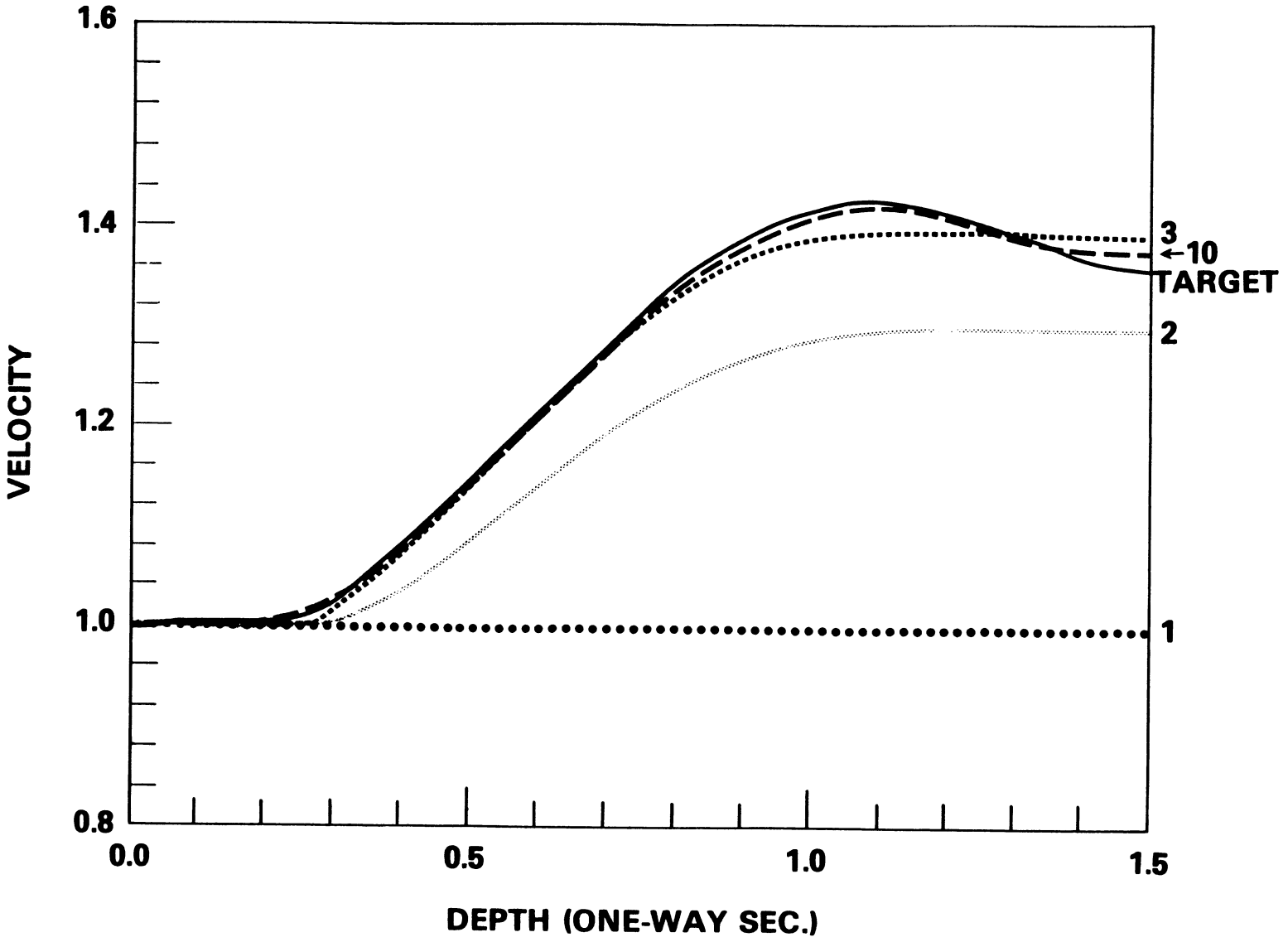
1.6
1.4
1.2
1.0
0.8
VELOCITY
0.0
0.5
1.0
1.5
DEPTH (ONE-WAY SEC.)
3
←10
TARGET
2
1

FIGURE 7B

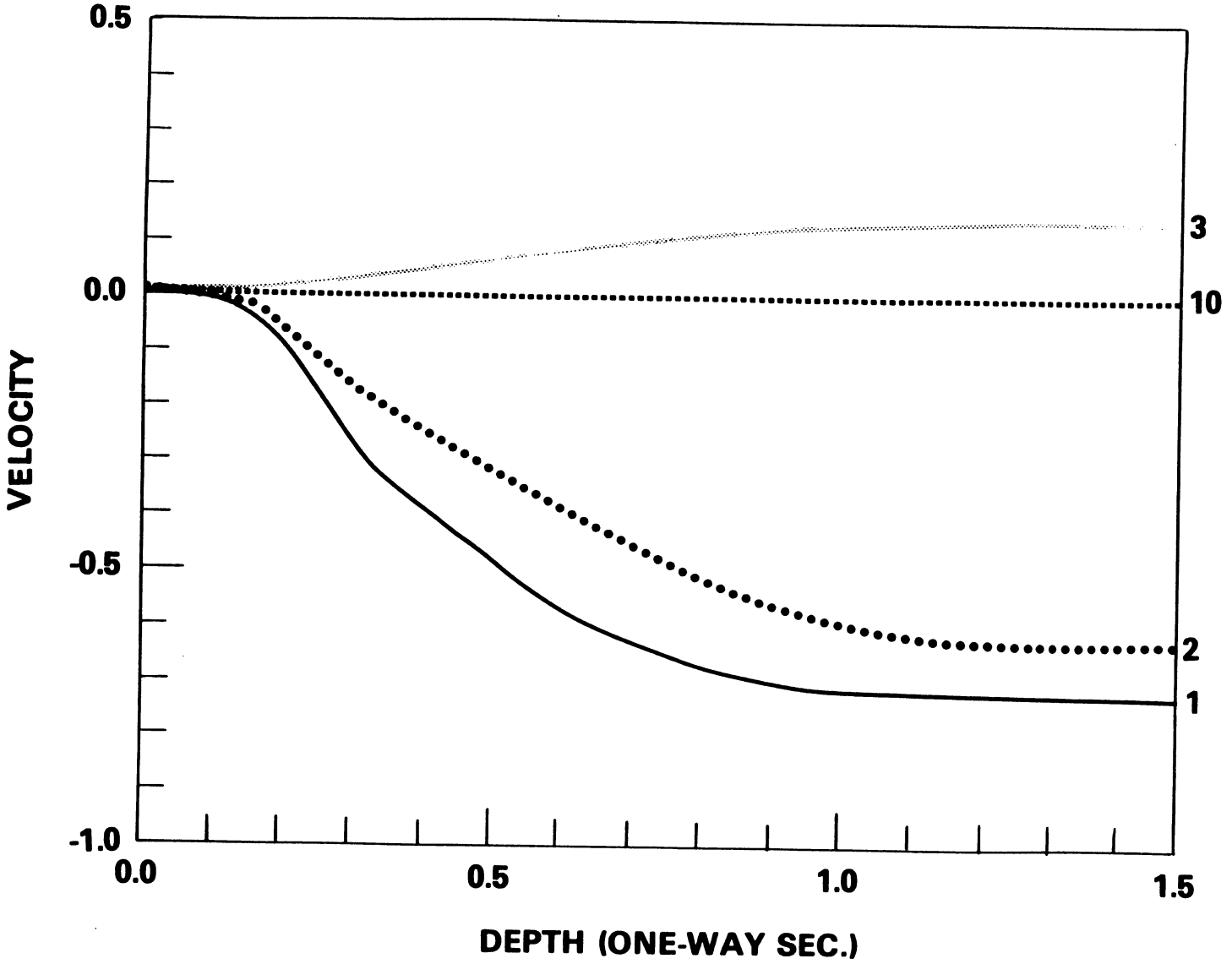

FIGURE 8A

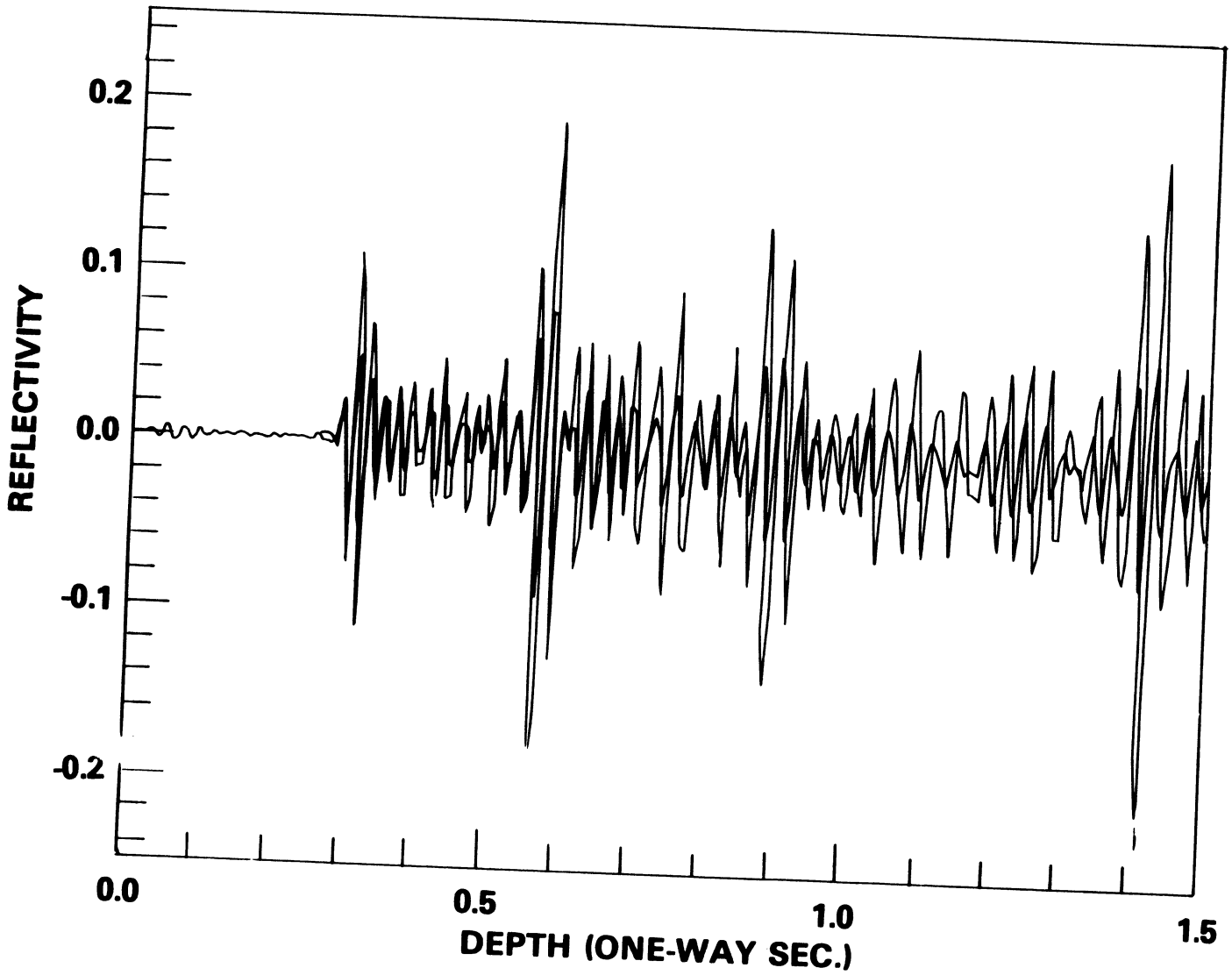

FIGURE 8B

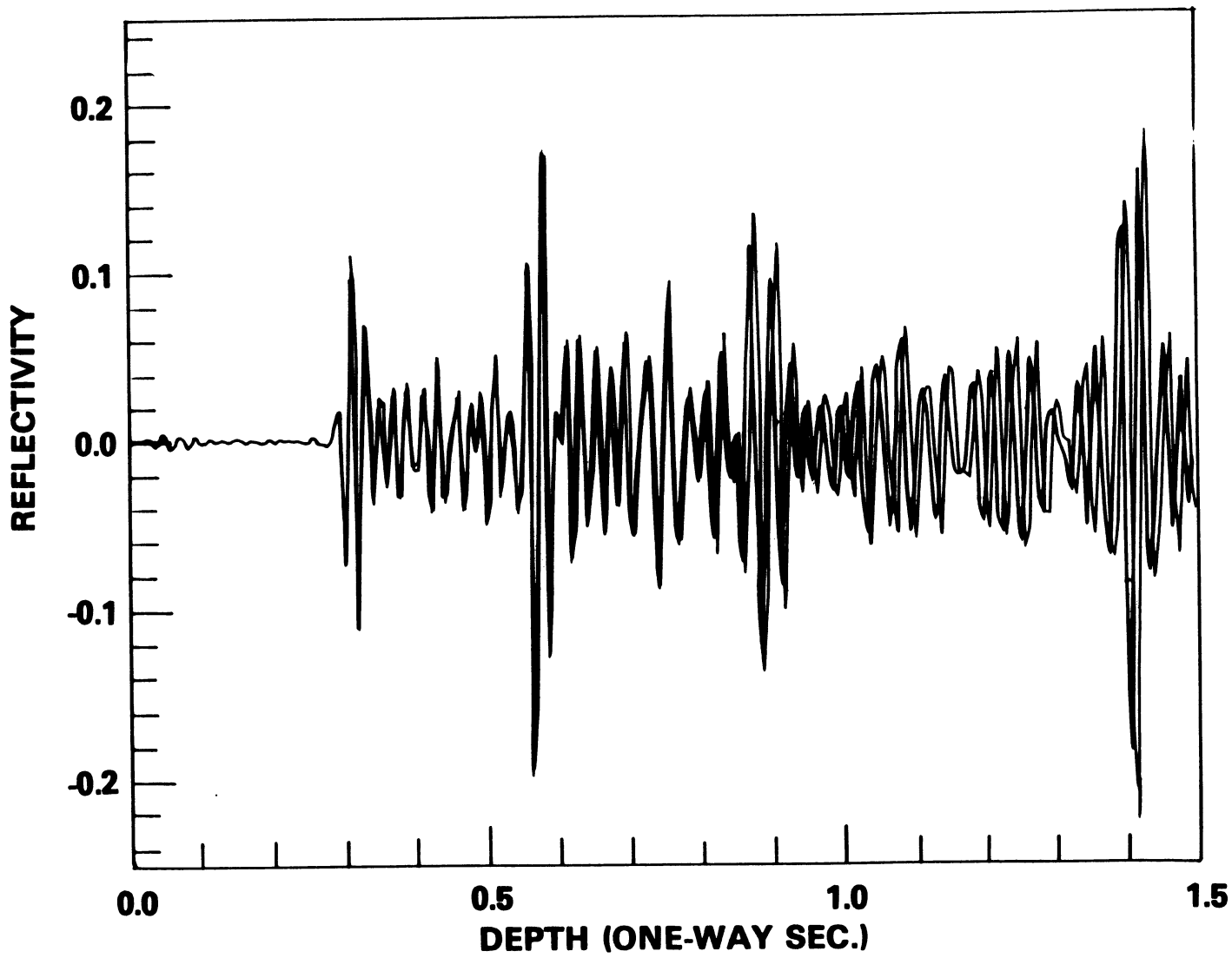

FIGURE 9

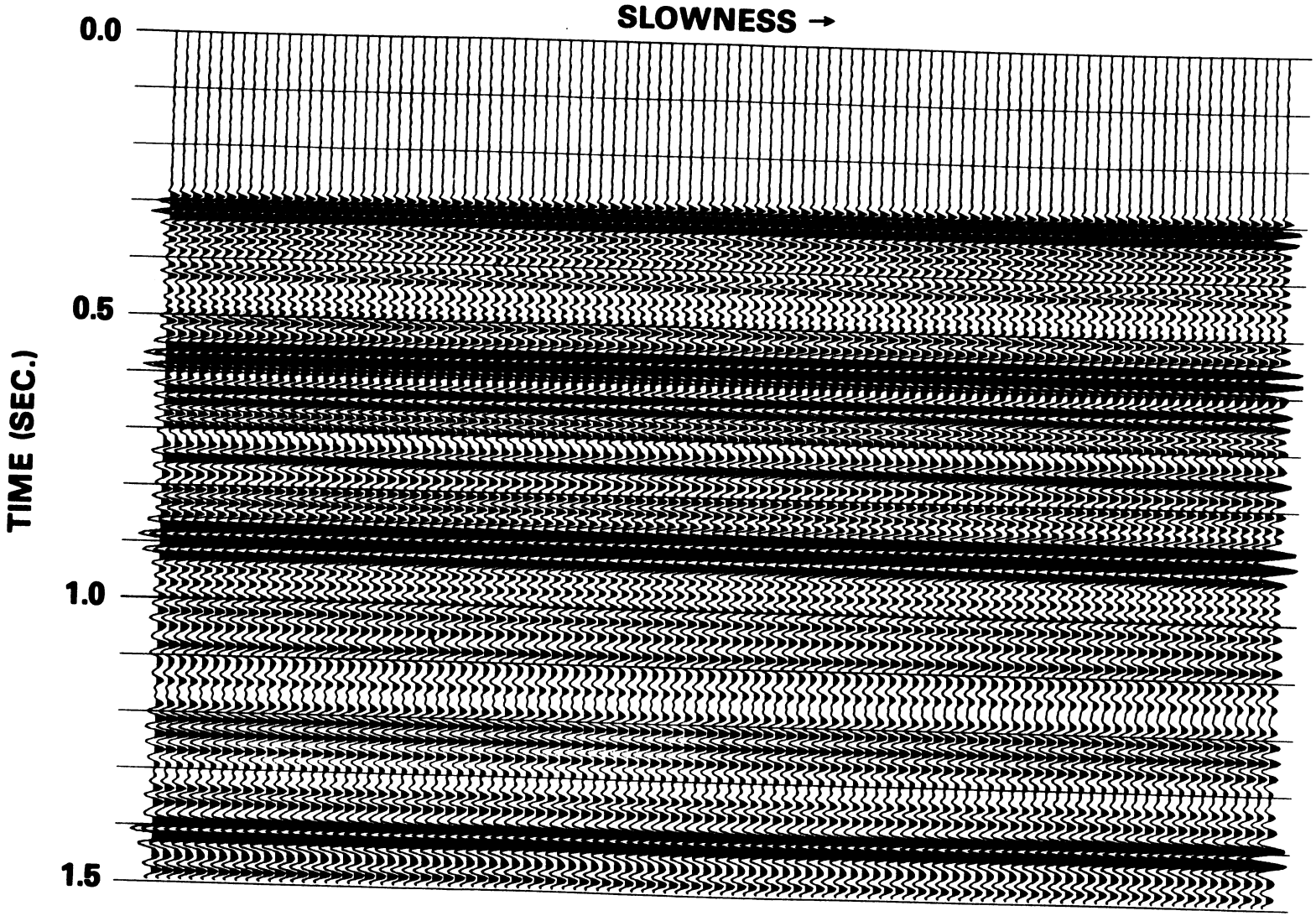

FIGURE 10

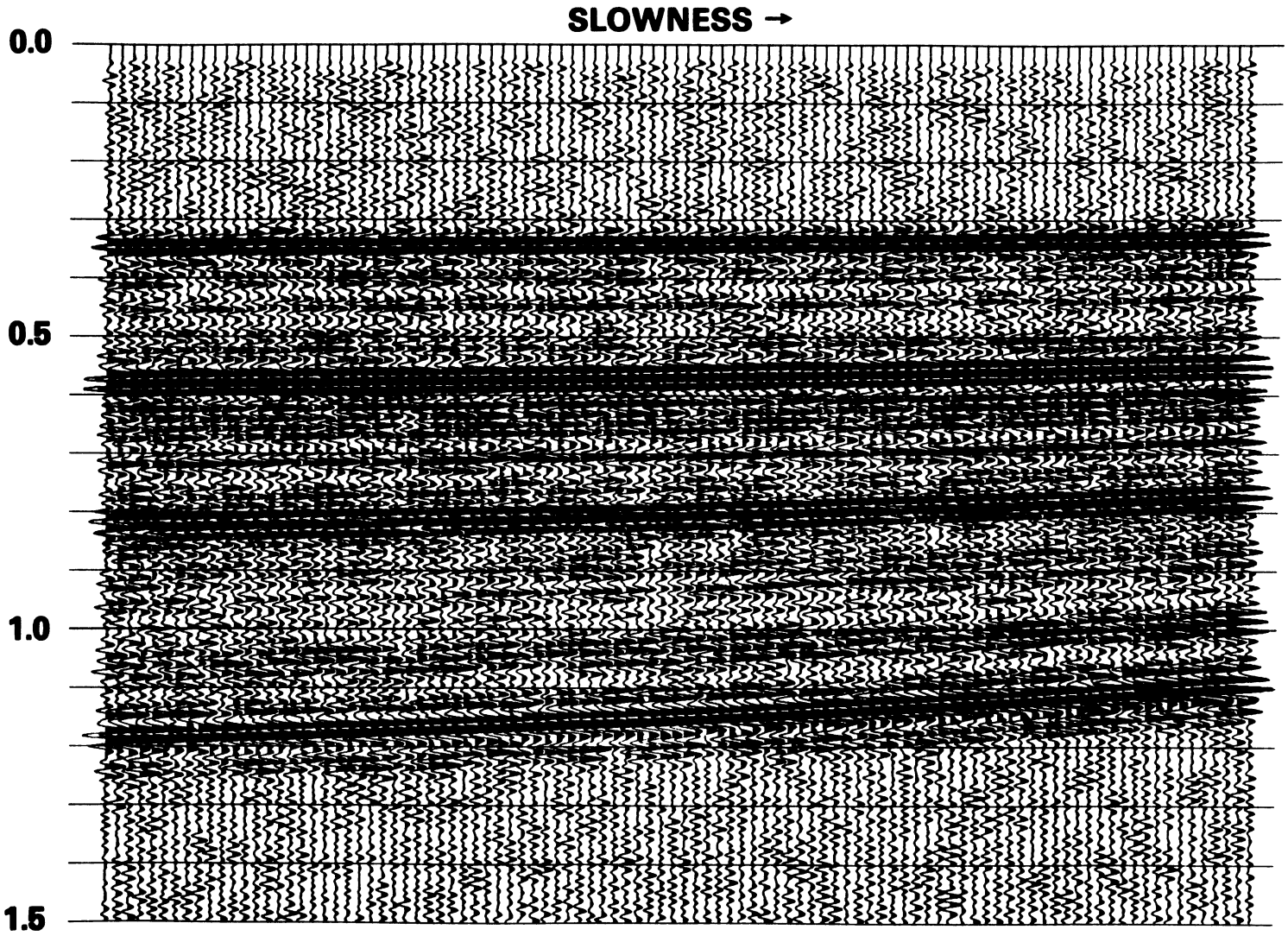

FIGURE 11

TARGET, 0% VS. 50% RMS NOISE

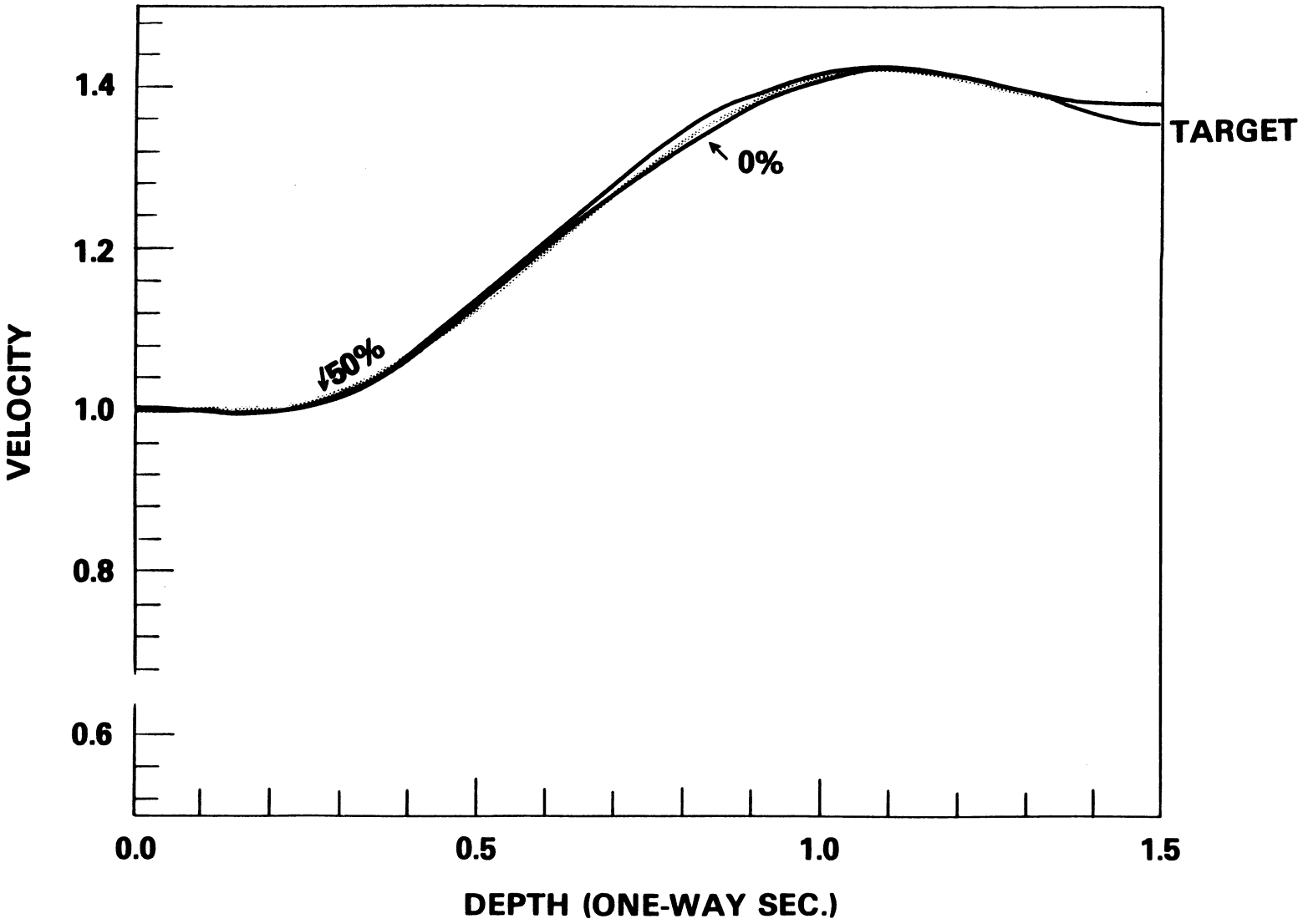

FIGURE 12

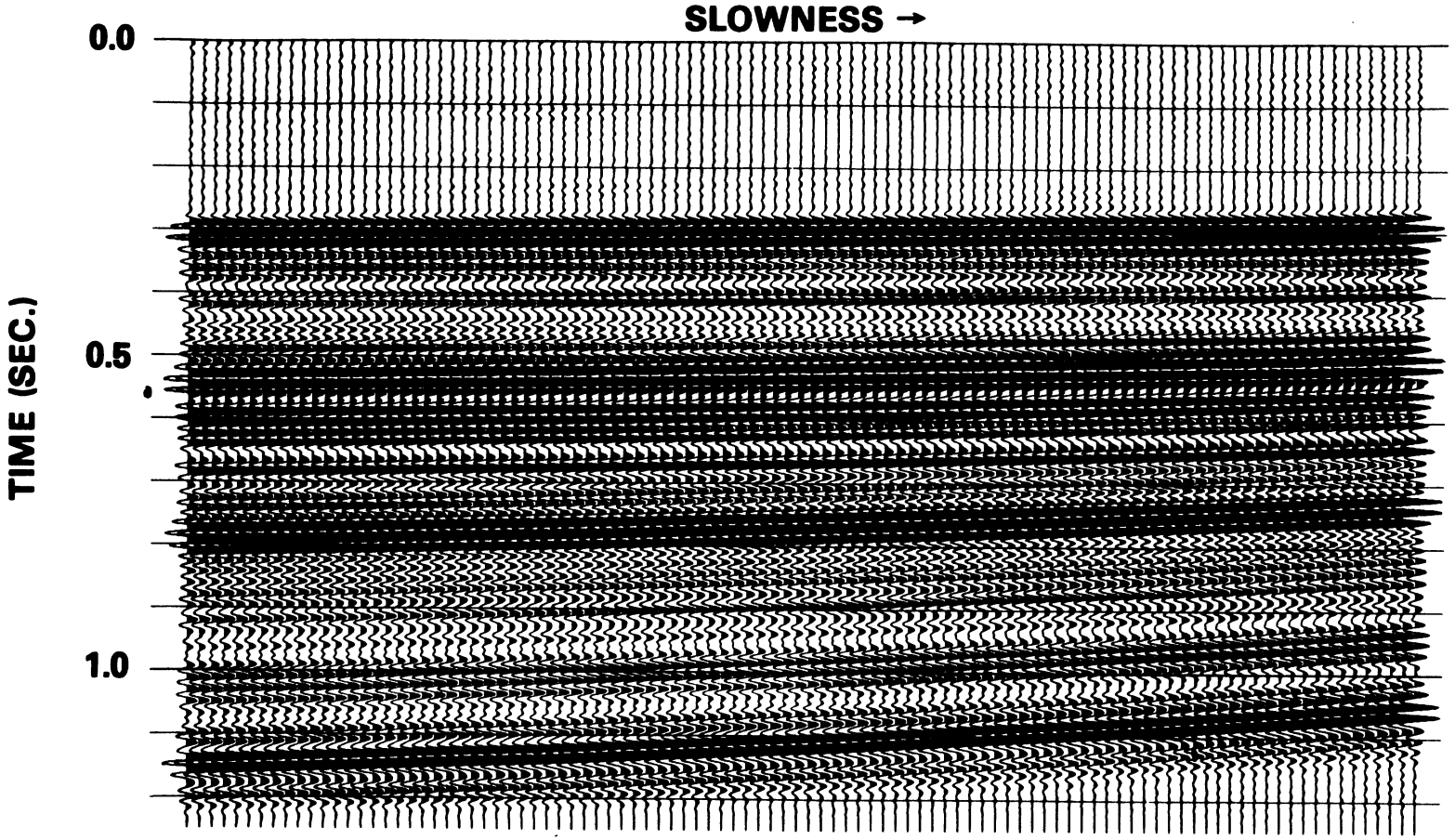

FIGURE 13

CDP STACK
GULF OF MEXICO

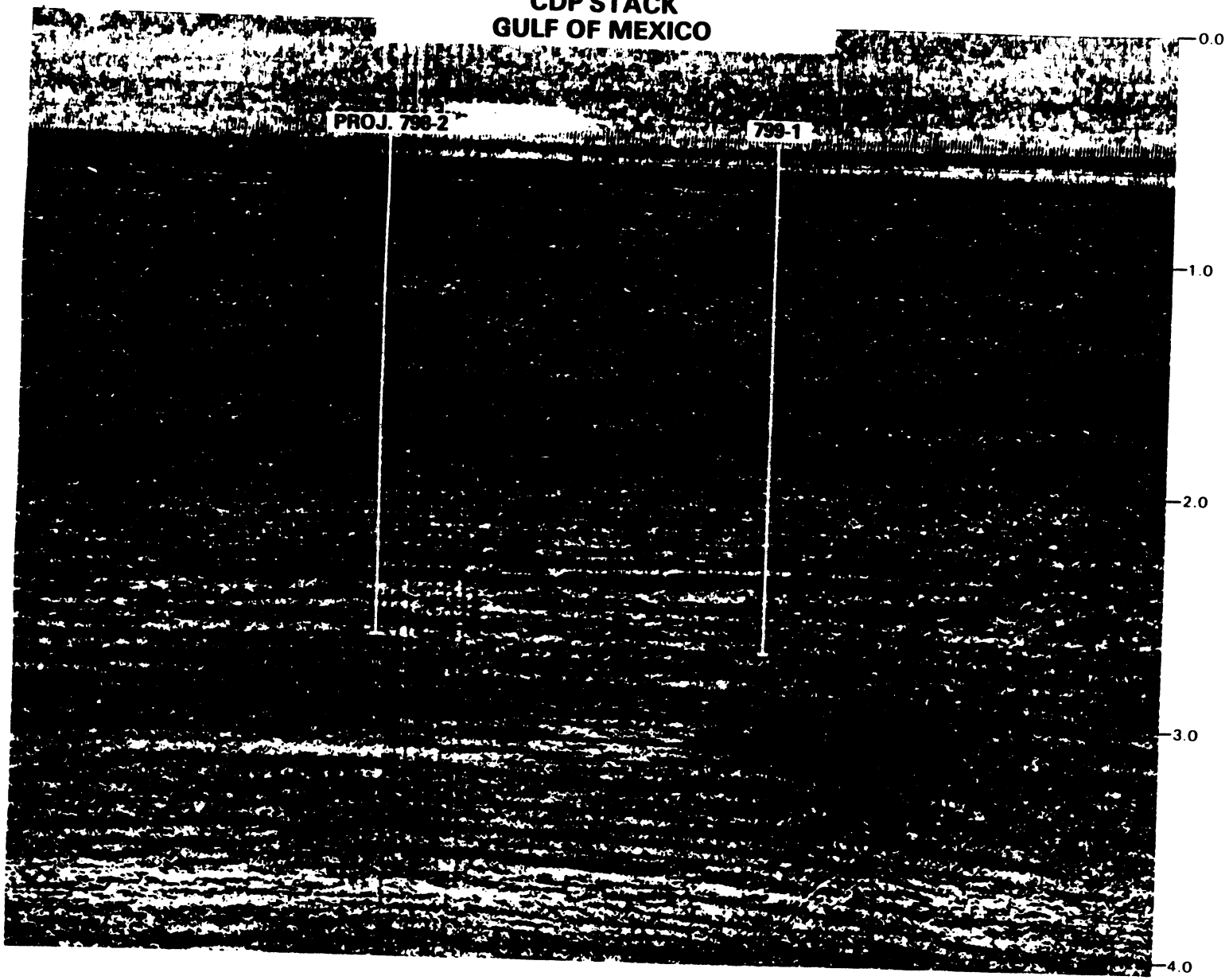

FIGURE 14
P-TAU DOMAIN MIDPOINT GATHER

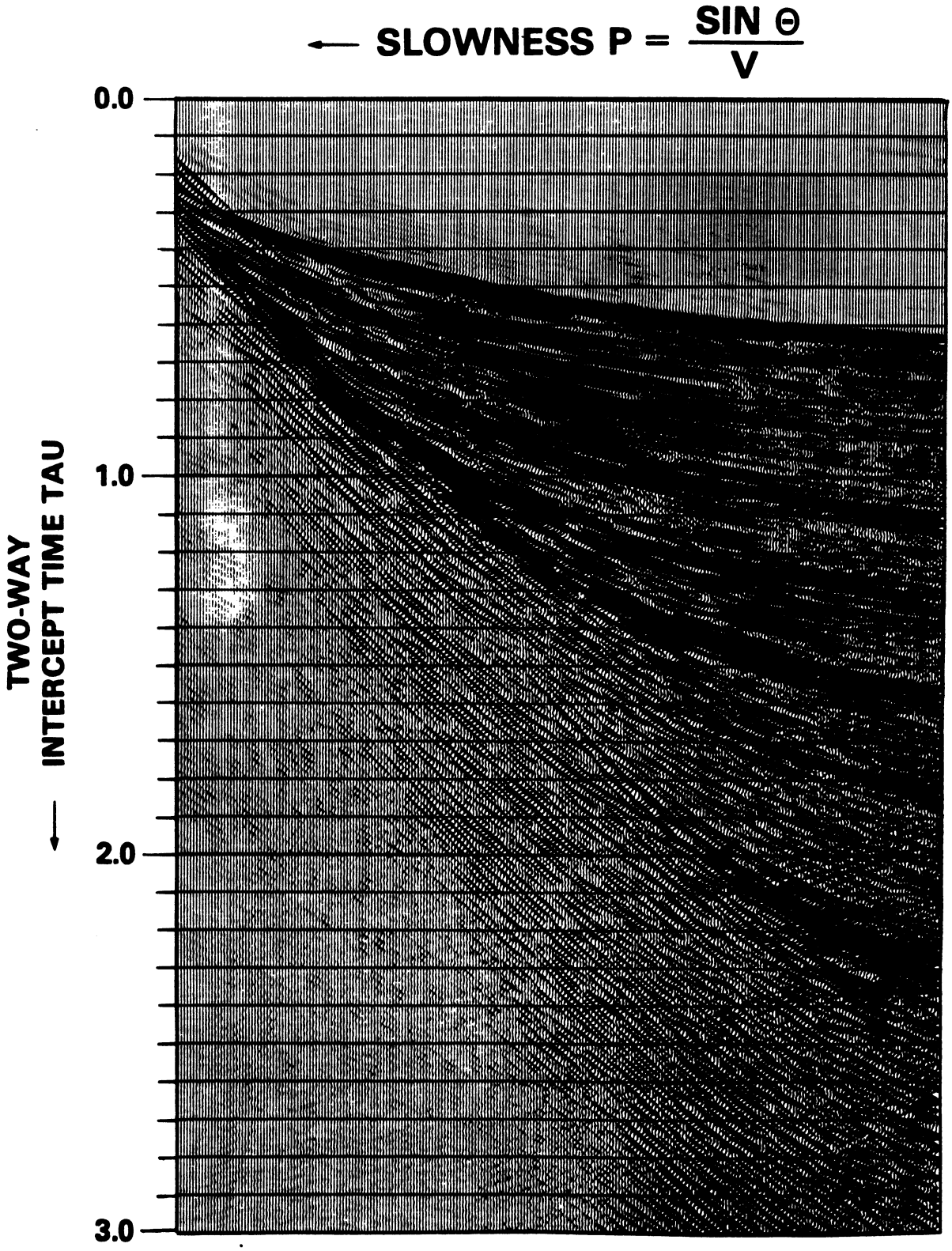

FIGURE 15

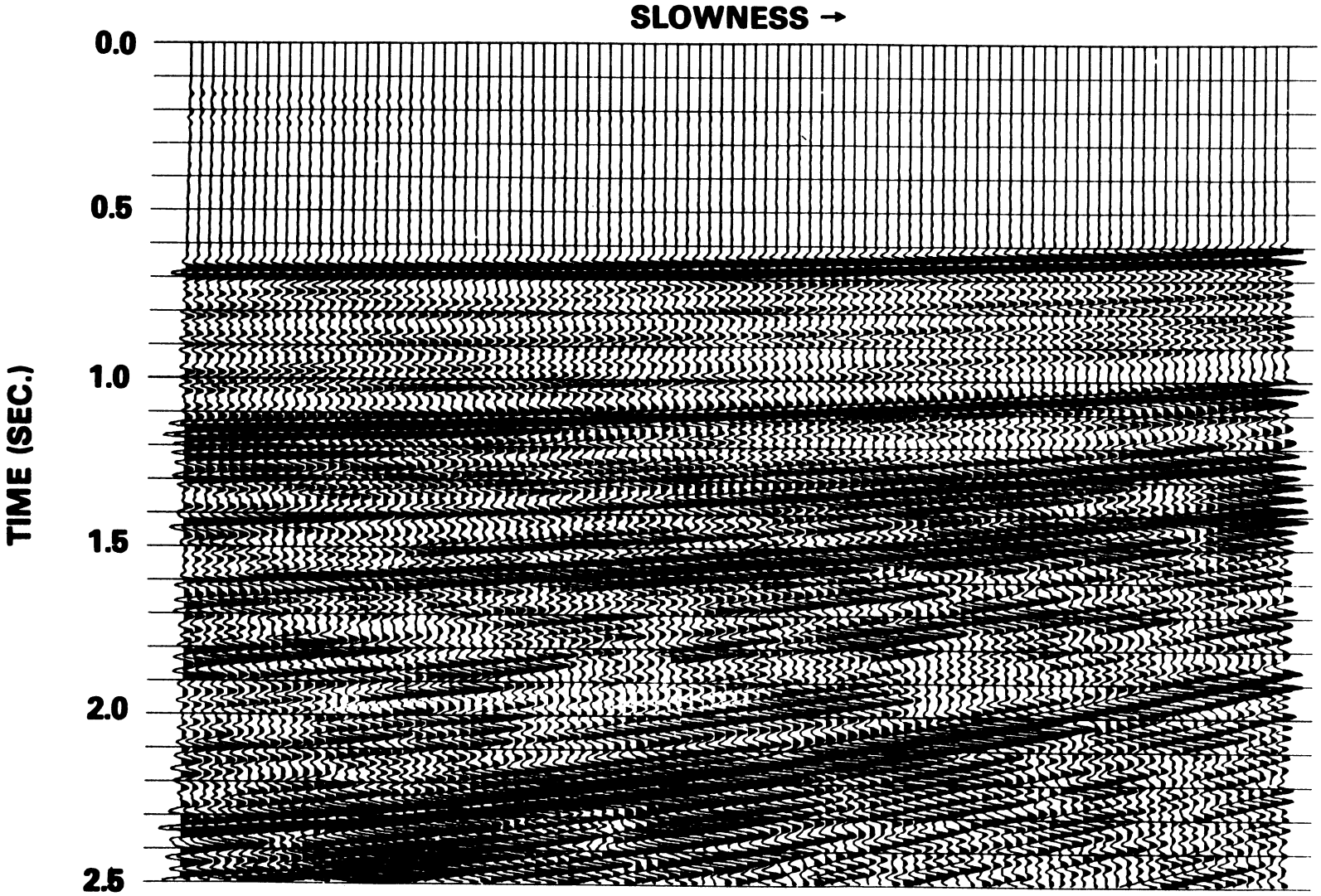

FIGURE 16

CM: TEST 1 VS. SONIC LOG

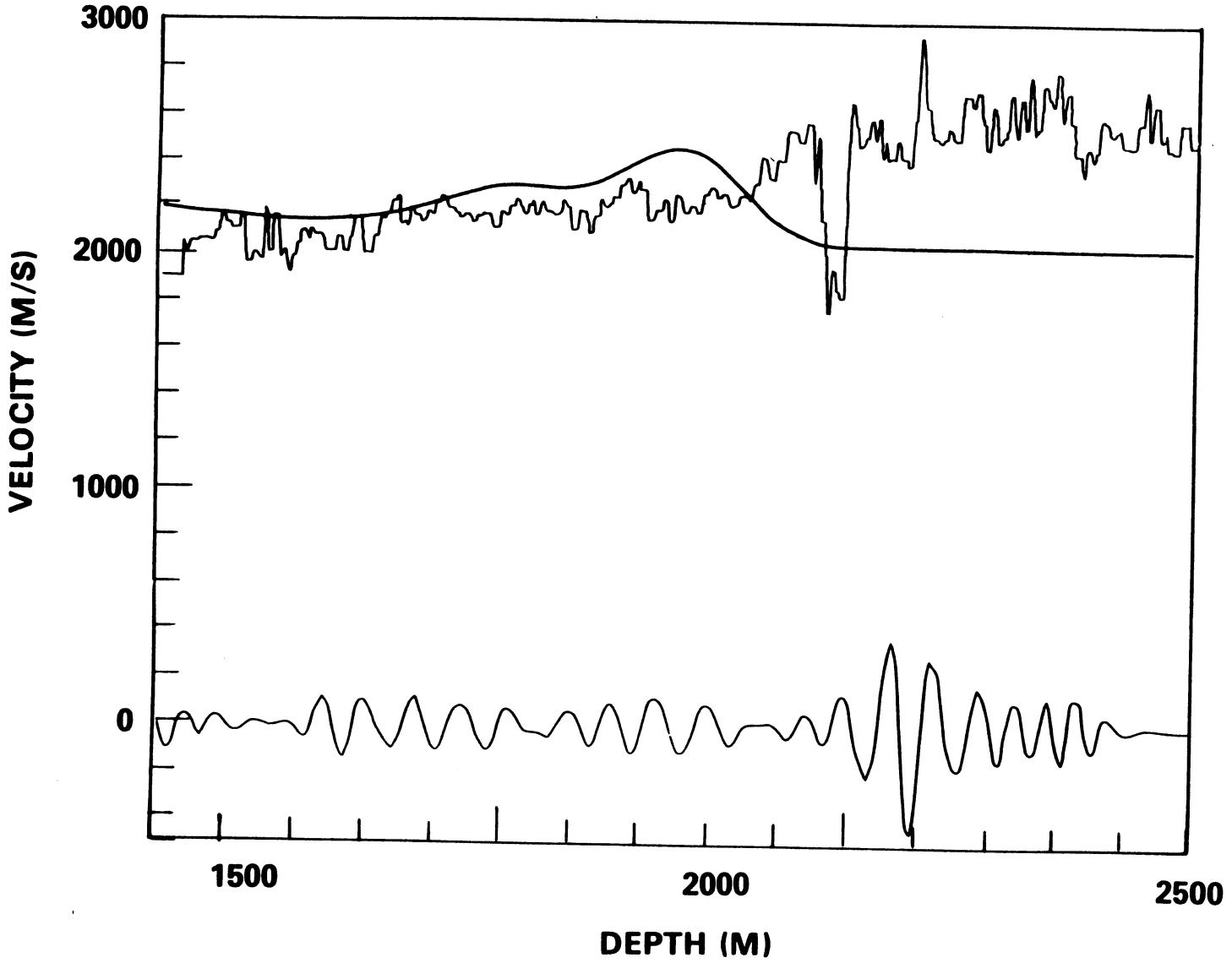

FIGURE 17